Journal of Medicinal Chemistry

pubs.acs.org/jmc

Article

Discovery of Novel, Potent, and Orally Bioavailable SMARCA2 Proteolysis-Targeting Chimeras with Synergistic Antitumor Activity in Combination with Kirsten Rat Sarcoma Viral Oncogene Homologue G12C Inhibitors

Sasikumar Kotagiri, Yawen Wang, Yanyan Han, Xiaobing Liang, Nicholas Blazanin, Hira Mazhar, Manu Sebastian, Phuong Kieu Nguyen, Yongying Jiang, and Yonathan Lissanu*

Cite This: *J. Med. Chem.* 2025, 68, 9202−9219

Read Online

ACCESS | Metrics & More | Article Recommendations | Supporting Information

ABSTRACT: Cancer genomic studies have identified frequent mutations in subunits of the SWI/SNF chromatin remodeling complex, including *SMARCA4* in nonsmall cell lung cancer with a frequency of up to 33% in advanced-stage disease, making it the most frequently mutated complex. We and others have identified *SMARCA2* to be synthetic lethal to *SMARCA4,* indicating that SMARCA2 is a high-value therapeutic target. Here, we disclose the discovery and characterization of potent, selective, and orally bioavailable cereblon-based SMARCA2 PROTACs. Biochemically, we showed that YDR1 and YD54 are potent SMARCA2 degraders. Further, we showed the antitumor growth inhibitory activity of YDR1 and YD54 in *SMARCA4* mutant xenografts. Finally, we show that YDR1 and YD54 synergize with the KRAS G12C inhibitor sotorasib to inhibit the growth of *SMARCA4* and *KRAS G12C* comutant lung cancer cells. These findings provide evidence for the utility of single agent or combination regimens containing SMARCA2 PROTACs as synthetic lethal therapeutics against *SMARCA4* mutant cancers.

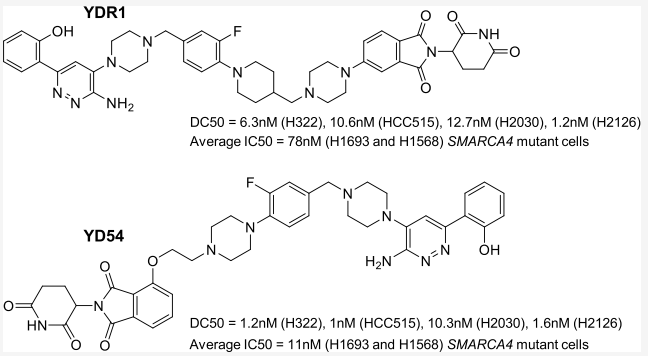

INTRODUCTION

A major discovery of large-scale cancer genomic studies is the identification of frequent mutations in subunits of the SWI/SNF (switch/sucrose non-fermenting) chromatin remodeling complex, including *SMARCA4* (also known as *BRG1*) and *ARID1A*, ranging from 16% in early-stage disease to 33% in advanced lung cancer.[1−7] Additionally, a meta-analysis of 44 cancer genomic studies has shown that 20% of all solid tumors have mutations in subunits of the SWI/SNF complex, making it one of the most frequently mutated complexes in cancer.[6] The SWI/SNF complex is a large multisubunit complex that uses ATP hydrolysis to remodel nucleosomes and enable chromatin-dependent processes such as transcription, DNA repair, and replication.[8,9] SMARCA2 (also known as BRM) and SMARCA4 are mutually exclusive core catalytic subunits with ATPase enzymatic activity. Mutations in *SMARCA4* are inactivating and cannot be directly targeted therapeutically. Thus, there is an intense effort to identify synthetic lethal or other vulnerabilities in *SMARCA4* mutants. While several studies have reported enhanced sensitivity of *SMARCA4* mutant lung cancers to inhibition of oxidative phosphorylation (OXPHOS),[10] Aurora kinase A,[11] EZH2,[12] ATR,[13] and KDM6 methyltransferases,[14] none of these have progressed into clinical success. Importantly, we and others have identified that the paralog *SMARCA2* shows a synthetic lethal genetic interaction with *SMARCA4* in lung cancer cell lines, suggesting that it is a high-value therapeutic target.[15−20] SMARCA2 is composed of helicase-SANT-associated (HSA) domain, DEXDc, and Helicase domains (that together constitute the ATPase domain), Snf2 ATP coupling (SnAC) domain, and bromodomain. From these, the ATPase and bromodomains are readily amenable to small molecule inhibition. As anticancer agents, inhibitors targeting the bromodomain were found to be not efficacious, while those targeting the ATPase domain of SMARCA2 were not selective and associated with undesired off-target activities against other ATPases such as SMARCA4, highlighting the need for alternative approaches of targeting SMARCA2.[16,21] Proteolysis-targeting chimeras (PROTACs) have emerged as an innovative class of

Received: October 23, 2024
Revised: March 27, 2025
Accepted: March 28, 2025
Published: April 25, 2025

https://doi.org/10.1021/acs.jmedchem.4c02577
J. Med. Chem. 2025, 68, 9202−9219

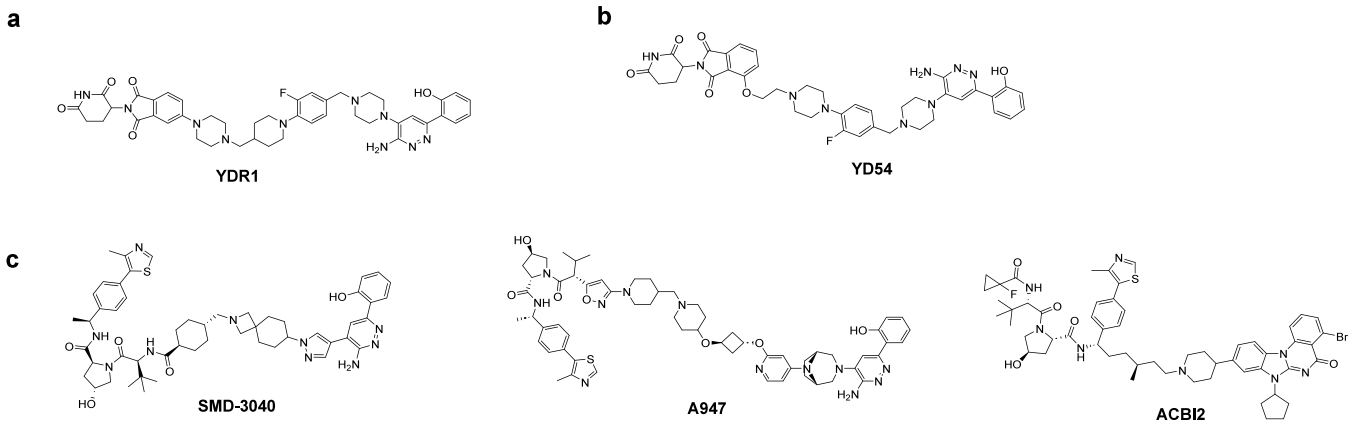

Figure 1. Structures of novel and recently reported SMARCA2 PROTACs. (a) YDR1, (b) YD54, and (c) SMD-3040, A947, and ACBI2.

Scheme 1. Synthesis of YD54

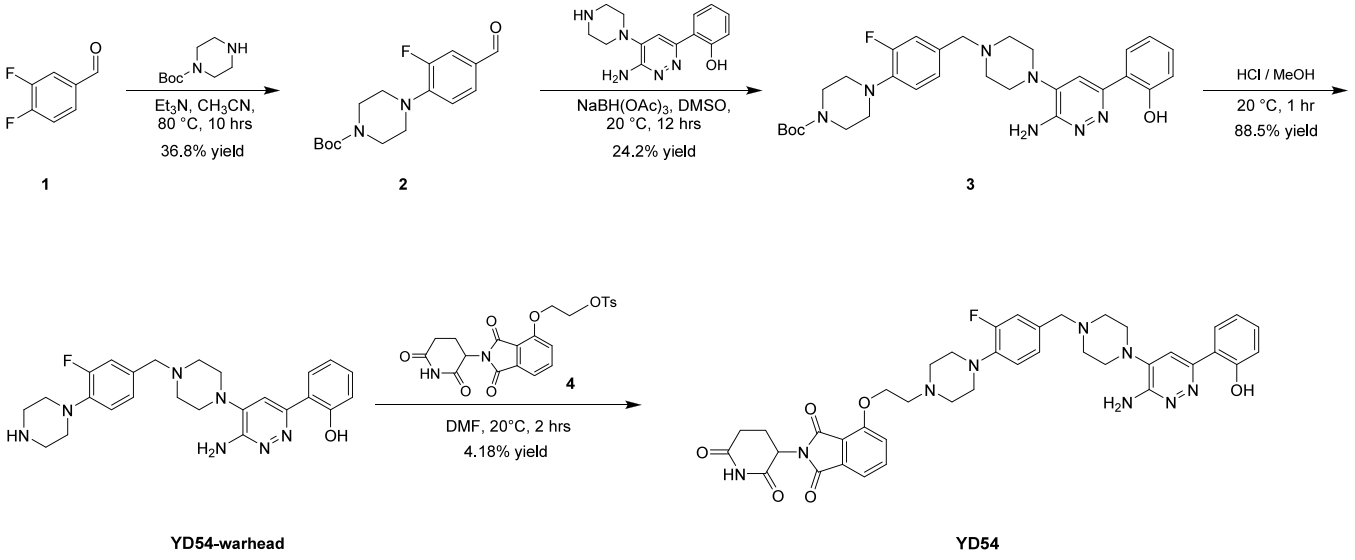

therapeutics to expand the repertoire of the targetable genome.[22] PROTACs are heterobifunctional molecules that tether a small molecule ligand of a protein of interest to an E3 ubiquitin ligase binder and result in induced proximity of a target protein to the cellular ubiquitination machinery leading to ubiquitination and proteasomal degradation of target protein.[22] Recently, several SMARCA2 PROTACs, including ACBI2, A947, and SMD-3040, have been reported with varying pharmacokinetic properties and a wide range of selectivity over SMARCA4[23−25] (Figure 1). While these developments are a major leap for the field, all these PROTACs utilize ligands to recruit the VHL E3 ubiquitin ligase. The only other PROTAC that targets SMARCA2 using cereblon E3 ligase is a dual SMARCA4 and SMARCA2 degrader which has higher selectivity to SMARCA4.[26] So far, VHL and cereblon are the most commonly utilized E3 ligases in PROTAC design. Importantly, cereblon-based PROTACs have advanced the most in clinical development including ARV-471 in Phase 3 clinical trials for breast cancer.[27] Furthermore, acquired resistance to PROTACs in cancer treatment in model systems was primarily caused by genomic alterations that disable core components of the E3 ligase utilized.[28] Thus, having an array of PROTACs that use different E3 ligases for any therapeutic target is highly desirable. As all the above-described selective SMARCA2 PROTACs were based on VHL ligase, we decided to pursue the development of cereblon-based SMARCA2 PROTACs. We recently reported the discovery and detailed functional characterization as well as elucidation of mechanism of action of a novel SMARCA2 PROTAC termed YD23. However, YD23 was metabolically labile and not orally bioavailable indicating significantly improved versions need to be generated.[29]

Here, we report the discovery of YDR1 and YD54, potent, selective, and orally bioavailable SMARCA2 degrading PROTACs based on the E3 ligase cereblon by conjugating a SMARCA2 bromodomain ligand to pomalidomide (E3 ligase ligand) through rigid chemical linkers (Figure 1). We show that YDR1 and YD54 potently degrade SMARCA2 and selectively inhibit the growth of *SMARCA4* mutant lung cancer cell lines. We characterized the microsomal stability and possible pathways of metabolic inactivation and importantly, we showed that YDR1 and YD54 are orally bioavailable with favorable pharmacokinetic properties for *in vivo* studies. We further showed that YDR1 and YD54 are potently active in mice and degrade SMARCA2 in various tissues and xenograft tumors. We also demonstrated that YDR1 and YD54 were well-tolerated in mice and able to inhibit the growth of

https://doi.org/10.1021/acs.jmedchem.4c02577
J. Med. Chem. 2025, 68, 9202−9219

Scheme 2. Synthesis of YDR1

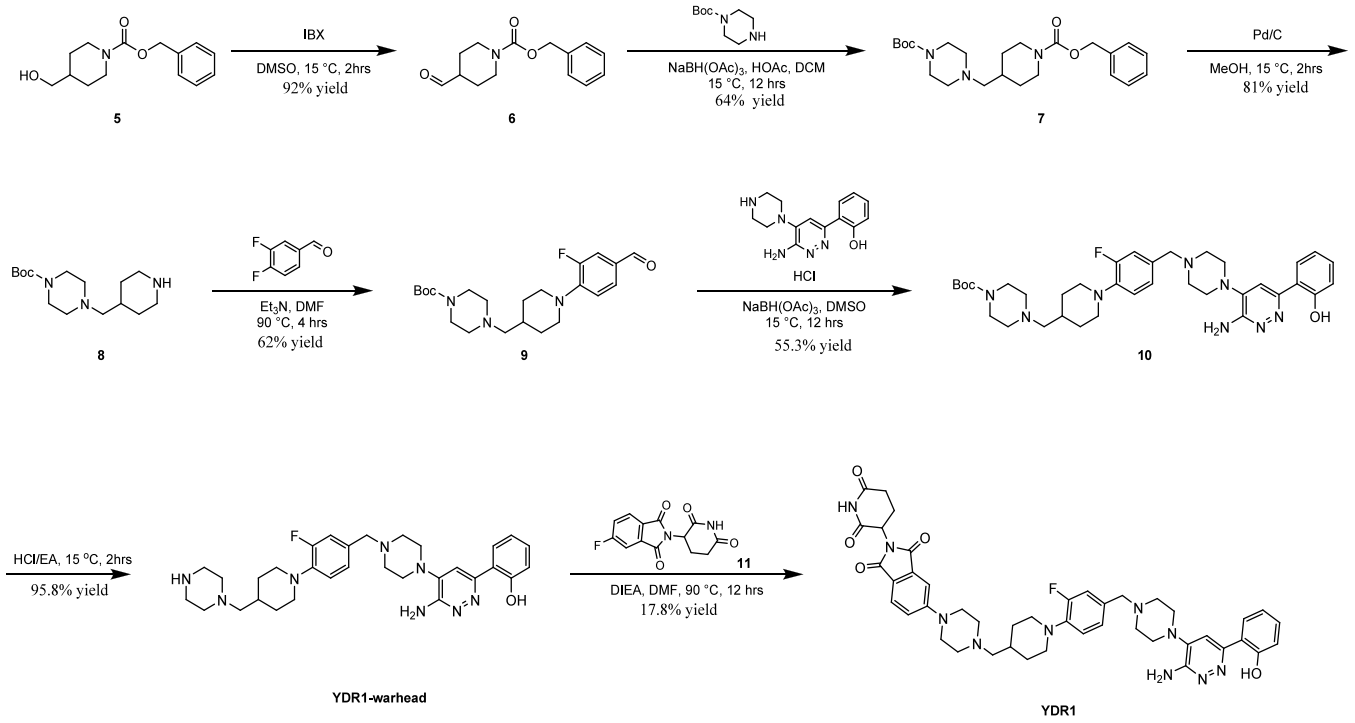

SMARCA4 mutant xenograft tumors. Finally, we showed that YDR1 and YD54 have a synergistic growth inhibitory effect in combination with the KRAS G12C inhibitor sotorasib in inhibiting the growth of *SMARCA4* and $KRAS^{G12C}$ comutant cells *in vitro* and xenograft tumors *in vivo*. To our knowledge, these are the first orally bioavailable cereblon-based selective SMARCA2 PROTACs. In summary, this report provides novel SMARCA2 PROTACs as chemical probes to interrogate the *in vitro* and *in vivo* functions of SMARCA2 and serve as potential drug leads for *SMARCA4* mutant cancers.

RESULTS

PROTAC Design. A series of heterobifunctional PROTACs targeted at SMARCA2 were designed based on the bromodomain binding ligand Gen-1 that was identified from a series of 2-(6-aminopyridazin-3-yl) phenols.[17,30] Further, the compounds were based on pomalidomide and designed to recruit the E3 ubiquitin ligase cereblon (CRBN). We have synthesized heterobifunctional compounds a) YDR1 and b) YD54 using variable fluorophenyl containing piperidinyl-piperazine or piperazine linkers respectively based on encouraging recent reports that such rigid linkers can help improve aqueous solubility, cell permeability and improve pharmacokinetic properties of the degrader (Figure 1).[31−33] While our discovery efforts also included testing flexible PEG or alkyl linkers as well as rigid alkyne or urea-based linkers, linkers with nitrogen-containing heterocycles performed better in imparting potency (Figure 1 and Supplementary Figure 1).

Chemistry. The synthesis of **YD54** and **YDR1** are shown in Schemes 1 and 2, respectively.

Synthesis of YD54. Intermediate **2** was prepared from 3,4-difluorobenzaldehyde and Boc-protected piperazine using an SN2 reaction. Following reductive amination with 2-(6-amino-5-(piperazin-1-yl) pyridazin-3-yl) phenol resulted in intermediate **3**. The **YD54 warhead** was subsequently obtained by Boc-deprotection of intermediate **3**. The E3 ligase ligand, intermediate **4**, was purchased from LabNetwork. **YD54** was obtained by SN2 reaction between **YD54 warhead** and intermediate **4**.

Synthesis of YDR1. Intermediate **6** was obtained by the oxidation of alcohol in intermediate **5** to aldehyde, followed by reductive amination with Boc-protected piperazine to make intermediate **7**. The −Cbz group in intermediate **7** was deprotected using hydrogenation to offer intermediate **8**, followed by SNAr reaction with 3,4-difluorobenzaldehyde to prepare intermediate **9**. Another reductive amination was performed between intermediate **9** and 2-(6-amino-5-(piperazin-1-yl) pyridazin-3-yl) phenol to generate intermediate **10**. **YDR1 warhead** was obtained via Boc-deprotection of intermediate **10**. The E3 ligase ligand intermediate **11** was purchased from LabNetwork, and the **YDR1** was obtained by SNAr reaction between **YDR1 warhead** and intermediate **11**.

Biological Activity. We have comprehensively investigated the biochemical and cellular effects of YDR1 and YD54 on *SMARCA4* WT and mutant lung cancer cell lines. Initially, we treated H1792, a *SMARCA4*-WT human lung cancer cell line with 1 nM to 10 μM of YDR1 and YD54 for 24 and 48 h. YDR1 degraded SMARCA2 in H1792 cells with a half-maximal degradation concentration (DC_{50}) of 69 nM at 24 h and 60 nM at 48 h while achieving a maximal degradation (D_{max}) of 87% at 24 h and 94% at 48 h (Figure 2a). YD54 degraded SMARCA2 in H1792 cells with DC_{50} of 8.1 nM at 24 h and 16 nM at 48 h. YD54 had a D_{max} of 98.9% at 24 h and 99.2% at 48 h. (Figure 2b). Importantly, YDR1 has only a moderate impact on SMARCA4 at 24 h with DC_{50} of 135 nM and D_{max} of 79% and at 48 h with DC_{50} of 381 nM and D_{max} of 69% (Figure 2a). YD54 has more impact on SMARCA4 at 24 h with DC50 of 19 nM and Dmax of 98% but becomes moderate at 48 h with DC_{50} of 149 nM and D_{max} of 99.3% (Figure 2b). Furthermore, we performed time course experiments to determine the kinetics of SMARCA2 degradation and found that YD54 has a more potent and faster onset of activity

https://doi.org/10.1021/acs.jmedchem.4c02577
J. Med. Chem. 2025, 68, 9202−9219

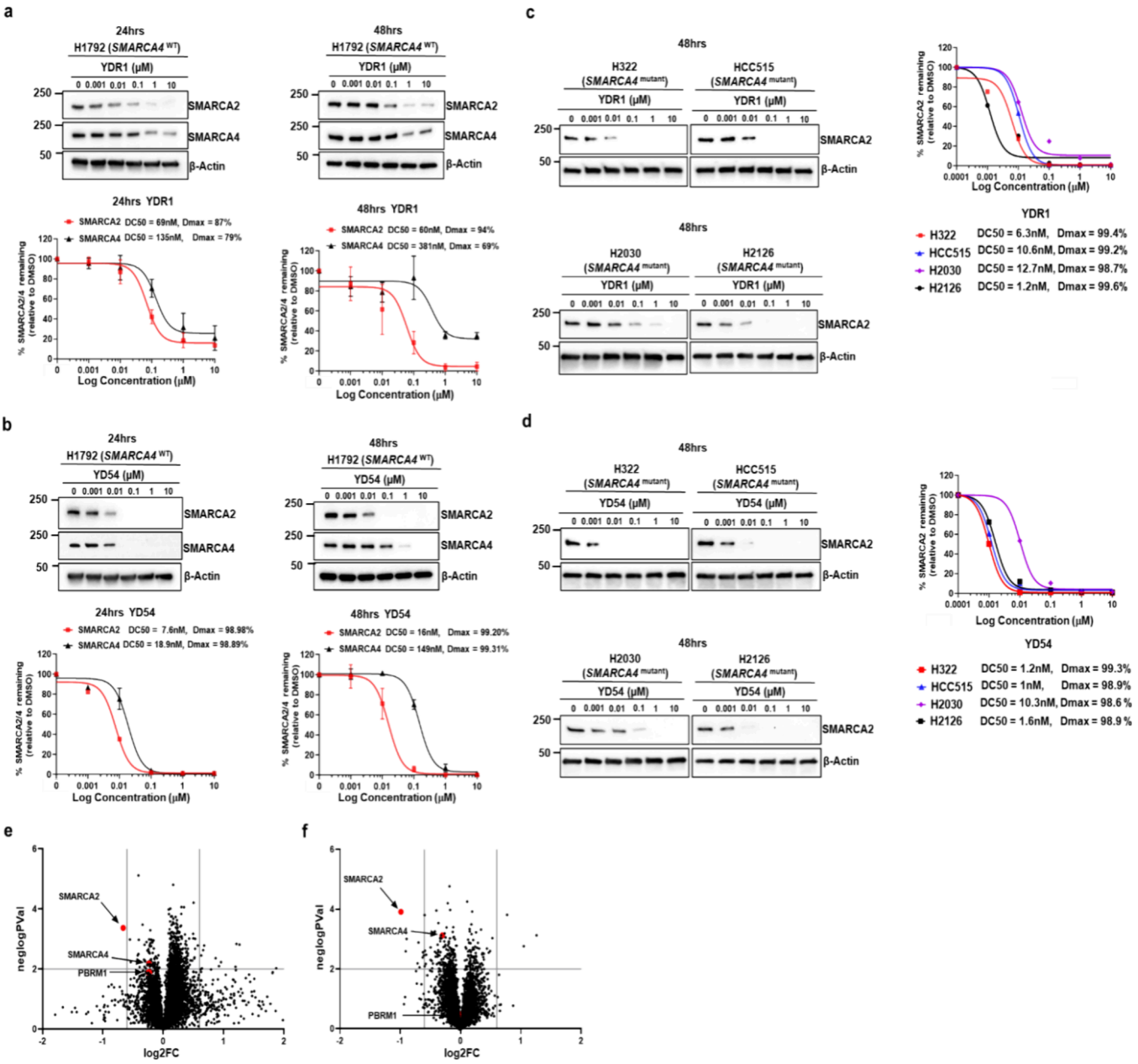

Figure 2. YDR1 and YD54 biological activity. (a) Immunoblot analysis of SMARCA2 and SMARCA4 protein levels in H1792 *SMARCA4*-WT cells treated with YDR1, as indicated (upper panels), and their quantification. Individual DC_{50} values were determined from $n = 3$ biological replicates (lower panels). Data was normalized with β-actin and presented as mean ± SEM. (b) Immunoblot analysis of protein levels in H1792 cells treated with YD54, as indicated (upper panels) and their quantitation. Individual DC_{50} values were determined from $n = 3$ biological replicates. Data was normalized with β-actin and presented as mean ± SEM. Immunoblot analysis of SMARCA2 in H322, HCC515, H2030, and H2126 *SMARCA4* mutant cell lines treated with (c) YDR1 and (d) YD54 as indicated (right panels) and their quantification after normalization with β-actin. (e) Scatterplots of quantitative TMT mass spectrometry of global proteome following 48 h treatment with 100 nM YDR1 in H1792 *SMARCA4*-WT cell line. (f) Scatterplots of quantitative TMT mass spectrometry of global proteome following 24 h treatment with 20 nM YD54 in H1792 *SMARCA4*-wild type cell line.

while both compounds continue to have robust degradation up to 96 h post-treatment (Figure S2a,b). To further expand the investigation on the potency of YDR1 and YD54 on additional *SMARCA4* mutant cell lines, we treated H322, HCC515, H2030, and H2126 cell lines with YDR1 and YD54. YDR1 potently degraded SMARCA2 in H322, HCC515, H2030, and H2126 cell lines with a half-maximal degradation concentration (DC_{50}) of 6.4 nM, 10.6 nM, 12.7 nM and 1.2 nM respectively while achieving profound maximal degradation (D_{max}) of 99.2%, 99.4%, 98.7% and 99.6% (Figure 2c). Similarly, YD54 potently degraded SMARCA2 in H322, HCC515, H2030, and H2126 cell lines with a half-maximal degradation concentration (DC_{50}) of 1 nM, 1.2 nM, 10.3 nM and 1.6 nM respectively while achieving a maximal degradation (D_{max}) of 99.3%, 98.9%, 98.6% and 98.9% (Figure 2d). Taken together, these data show that YDR1 and YD54 are highly potent SMARCA2 degraders. Next, we sought to determine whether YDR1 and YD54 are working as bona fide PROTACs and performed various rescue experiments. First, we performed standard competition assays using small molecules constituents

https://doi.org/10.1021/acs.jmedchem.4c02577
J. Med. Chem. 2025, 68, 9202−9219

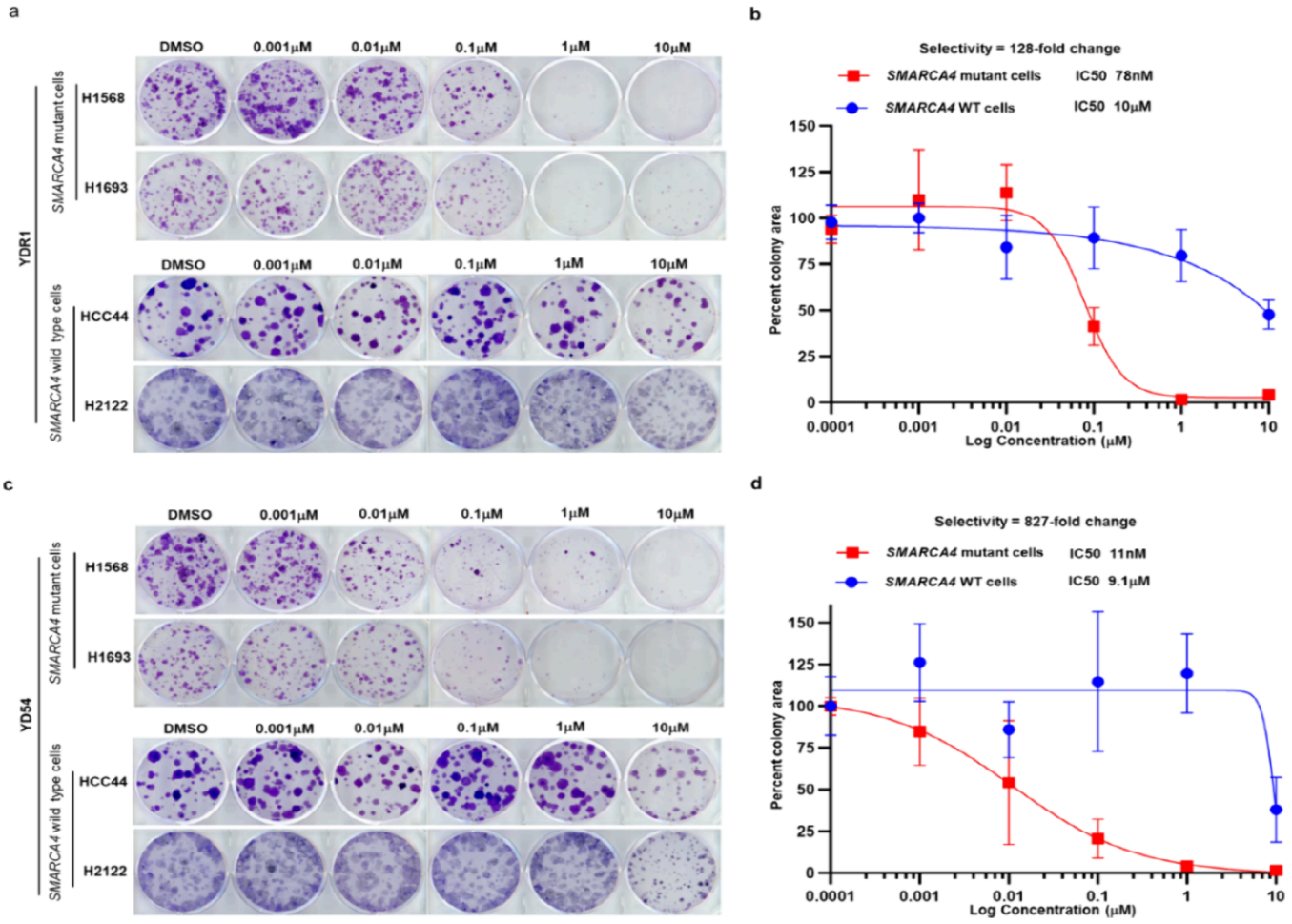

Figure 3. Selective growth inhibitory activity of YDR1 and YD54 in lung cancer cell lines. (a) Representative images of clonogenic growth assays in *SMARCA4* mutant cell lines and *SMARCA4*-WT cell lines treated with indicated concentrations of YDR1. (b) Quantitation of percent change in clonogenic area (relative to DMSO) as shown in (a). Error bars represent mean ± SEM from $n = 3$ biological replicates. (c) Representative images of clonogenic growth assays in *SMARCA4* mutant cell lines and *SMARCA4*-WT cell lines treated with indicated concentrations of YD54. (d) Quantitation of percent change in colonies area (relative to DMSO) as shown in (c). Error bars represent mean ± SEM from $n = 3$ biological replicates.

used in the making of SMARCA2 degraders. Gen-1 binds to the bromodomain of SMARCA2, and pomalidomide binds to cereblon. Thus, we used increasing concentrations of Gen-1 or Pomalidomide in competition assays with YDR1 or YD54 and showed profound rescue of SMARCA2 levels in a dose-dependent manner (Figure S2c,d). Further, we used MLN4924, an inhibitor of Neddylation (via inhibition of E1 NEDD8 activating enzyme), and showed rescue of SMARCA2 levels in a dose-dependent manner (Figure S2c,d). Additionally, we have used Bortezomib to inhibit proteosome and rescued SMARCA2 levels (Figure S2c,d). Finally, we have corroborated these pharmacologic rescue experiments using genetic approaches. Since YDR1 and YD54 are cereblon-based degraders, we have knocked out *cereblon* (*CRBN*) using CRISPR-Cas9 and investigated the effect of *CRBN* knockout in H322 cells. Importantly, we found that SMARCA2 protein levels are rescued in *CRBN* Knockout cells (Figure S2c,d). We also showed the cell growth phenotype rescue in *CRBN* knockout in H322 *SMARCA4* mutant cells treated by YDR1 and YD54 (Figure S2c,d). Taken together, this body of data strongly suggests that the compounds induce degradation of SMARCA2 in the classically accepted PROTAC fashion by E3 ligase-target protein-PROTAC ternary complex formation, ubiquitination, and via the proteasome.

Quantitative proteomics using tandem mass tag (TMT) has rapidly become a powerful approach to investigate the effect of degraders on the cellular proteome to identify targets and establish selectivity profiles. Hence, we treated the H1792 *SMARCA4*-wild type cell line with DMSO and 100 nM YDR1 for 48 h and performed TMT mass spectrometry. A total of 8626 proteins were reliably identified and quantified. Fold change and significance plot showed SMARCA2 was the only protein downregulated in YDR1 treated samples at a 1.5-fold change with a p-value of <0.05 showing remarkable selectivity of the compound (Figure 2e). A similar proteomics experiment was performed using YD54, where we observed that SMARCA2 is the most significantly and potently degraded protein, showing its remarkable selectivity. (Figure 2f). Importantly, SMARCA4 remained minimally altered at these conditions, again highlighting the relative selectivity of YDR1 and YD54 to SMARCA2 over SMARCA4. Our recently published manuscript showed that one of the key functional consequences of SMARCA2 degradation in *SMARCA4* mutant cancer cells is the modulation of the YAP signaling pathway.[34] Hence, we treated H322 *SMARCA4* mutant cells with YDR1

https://doi.org/10.1021/acs.jmedchem.4c02577
J. Med. Chem. 2025, 68, 9202−9219

Table 1. Comparison of Human and Mouse Liver Microsomal Metabolism of YDR1 and YD54

mouse microsomal assay						
compound	R2	$T_{1/2}$ (min)	Clint (mic) (μL/min/mg)	Clint (liver) (mL/min/kg)	remaining (T = 60 min)	remaining (NCF = 60 min)
YDR1	0.9545	59.733	23.203	91.88388	0.49976	0.93484
YD54	0.9544	45.949	30.164	119.44944	0.41402	0.36821
human microsomal essay						
compound	R2	$T_{1/2}$ (min)	Clint (mic) (μL/min/mg)	Clint (liver) (mL/min/kg)	remaining (T = 60 min)	remaining (NCF = 60 min)
YDR1	0.8751	58.024	23.887	21.4983	0.4743	0.33012
YD54	0.8957	34.876	39.741	35.7669	0.32336	0.50107

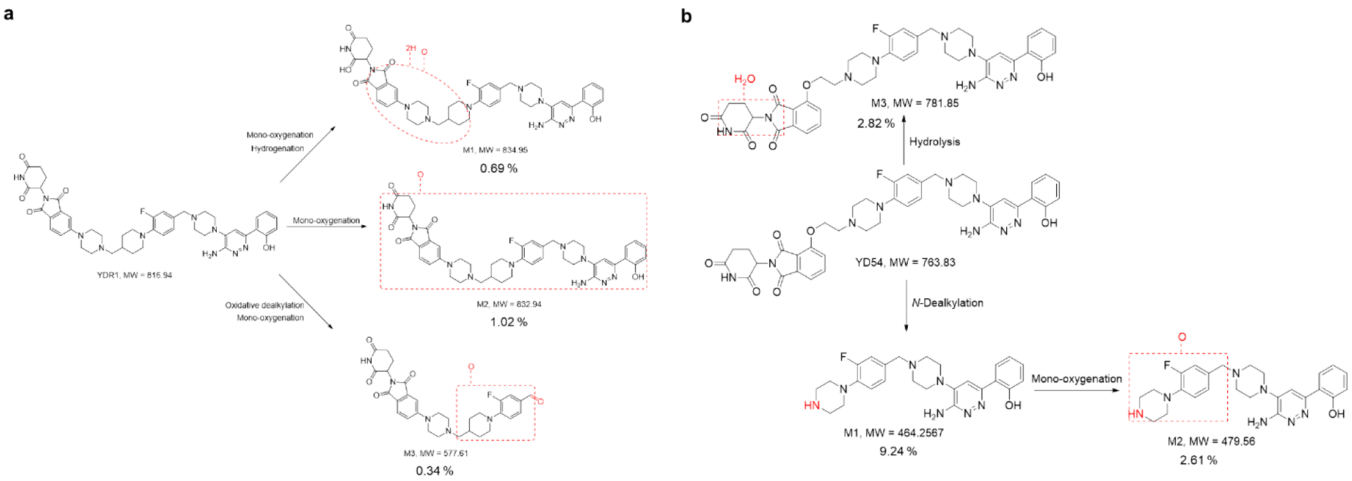

Figure 4. Metabolic stability and pathways of inactivation of YDR1 and YD54 in liver microsomal assays. YD54 and YDR1 of concentration 10 μM was incubated with mouse liver microsomes at 37 °C for 60 min, samples were analyzed by LC-UV-HRMS, and percentage of each metabolite structures were indicated. (a) YDR1 and (b) YD54.

or YD54 for 96 h and investigated the status of the YAP signaling pathway. We observed a drastic increase in phosphorylation of YAP1 levels at S109 residue. We also observed a potent increase in phosphorylation of YAP1 levels at S127 residue when H322 cells were treated with YDR1 or YD54 (Supplementary Figure 3a-b). These are known highly regulatory phosphorylation sites in YAP that result in its inactivation via various mechanisms, including changes in localization. While these results are consistent with our recent publication, our new compounds' effect sizes are more profound, most likely due to their superior potency.

YDR1 and YD54 Selectively Inhibit Growth of *SMARCA4* Mutant Lung Cancer Cell Lines. We next assessed the impact of YDR1 and YD54 on cellular growth by performing a 10-day clonogenic assay of two *SMARCA4* mutant cell lines (H1568 and H1693) and two *SMARCA4*-WT lung cancer cell lines (HCC44 and H2122). Both YDR1 and YD54 caused a dose-dependent inhibition in clonogenic assays in *SMARCA4* mutant cells (Figure 3a,c) with average cellular IC_{50} values of 78 and 11 nM, respectively (Figure 3b,d). Importantly, both YDR1 and YD54 had a minimal impact on the growth of *SMARCA4* WT cell lines with average cellular IC_{50} of 10 and 9.1 μM, respectively (Figure 3b,d). This implies about 128-fold and 827-fold activity of YDR1 and YD54, respectively, on *SMARCA4* mutant cells compared to WT cells, showing the remarkable selectivity of cellular phenotypic effect on mutants.

Metabolic Stability and Pathways of Inactivation of YDR1 and YD54 in Liver Microsomal Assays. For efficient activity, PROTACs need to induce the proximity of target protein and E3 ligase. An excess of E3 ligase binding ligand or protein of interest ligand can effectively compete for the formation of a ternary complex. A recent report highlighted metabolites of PROTACs that can potentially compete for binding to a ligand or E3 ligase to prevent full PROTAC-mediated degradation.[35] Hence, we were interested in exploring the stability and possible metabolites of YDR1 and YD54 and performed human and mouse liver microsomal stability assays followed by metabolite identification. YDR1 shows slow clearance with $T_{1/2}$ of 58 min, while YD54 shows moderate clearance with $T_{1/2}$ of 35 min in human microsomal assays (Table 1).

Similar trends were observed in mouse microsomal assays with YDR1 having a $T_{1/2}$ of 59 min and YD54 having 46 min (Table 1). We next sought to identify and characterize major metabolites of YDR1 and YD54 in mouse liver microsomes. Compounds at 10 μM were incubated with mouse liver microsomes at 37 °C for 60 min. After incubation, samples were analyzed by LC-UV-HRMS, and the structures of the metabolites were proposed based on the interpretation of their MS and MS^2 data. Under these experimental conditions, 3 metabolites were tentatively identified for YDR1 in mouse liver microsomes (Figure 4a). M1: mono-oxygenation and hydrogenation metabolite (P + O + 2H); M2: mono-oxygenation metabolite (P + O); M3: oxidative dealkylation and mono-oxygenation metabolite (P + O − $C_{14}H_{17}N_5O$ + O). In mouse liver microsomes, M2 was considered to be the top metabolite with a relative abundance of 1.02%. Similarly, under the

https://doi.org/10.1021/acs.jmedchem.4c02577
J. Med. Chem. 2025, 68, 9202−9219

current experimental conditions, 3 metabolites were tentatively identified for YD54 in mouse liver microsomes. M1: *N*-dealkylation metabolite (P − $C_{15}H_{12}N_2O_5$); M2: mono-oxygenation and *N*-dealkylation metabolite (P + O − $C_{15}H_{12}N_2O_5$); M3: hydrolysis metabolite (P + H_2O). In mouse liver microsomes, M1 was considered to be the top metabolite with a relative abundance of 9.24% (Figure 4b). These data suggest that minimal metabolite competition is expected in YDR1 while modest competition is expected from the dealkylation metabolite M1 in the case of YD54.

YDR1 and YD54 Are Orally Bioavailable. We next determined the bioavailability of YDR1 and YD54 after intraperitoneal (IP) or oral routes of administration. CD-1 mice were dosed with 25 mg/kg of YDR1 or YD54 in 0.5% methylcellulose/0.2% Tween 80 in water (for oral) or in 5% DMSO/5% solutol/90% water (for IP). Plasma was collected at 0.25, 0.5, 1, 2, 4, 8, and 24 h to know concentrations of YDR1 or YD54 by LC-MS/MS. Pharmacokinetic parameters are tabulated in Table 2. We observed robust oral bioavailability and stability of YDR1 with $T_{1/2}$ value exceeding 24 h (Table 2 and Figure 5, Supplementary Figure 4a). YD54 was also orally bioavailable with faster clearance as predicted from liver microsomal studies with $T_{1/2}$ of 6 h (Table 2 and Figure 5)

Table 2. Comparison of Intraperitoneal Injection and Oral Dosing of YDR1 and YD54 at 25 mg/kg

PK parameters	YDR1 P.O mean	YDR1 IP mean	YD54 P.O mean	YD54 IP mean
C_{max} (ng/mL)	649.3	1756.3	587.0	2039.7
$T_{1/2}$ (h)	ND	44.8	6.0	13.0
$AUC_{0\text{-last}}$ (ng h/mL)	12079.3	23213.7	4743.0	19365.3
$AUC_{0\text{-inf}}$ (ng h/mL)	ND	68813.0	5122.0	27108.3

Pharmacokinetic (PK) and Pharmacodynamic (PD) Correlation Studies of YDR1. After establishing basic PK profiles, we performed in-depth PK/PD correlation studies using Western blot quantification of *in vivo* levels of SMARCA2 as a key target engagement parameter. First, we administered vehicle control, 5 mg/kg, 10 mg/kg, 20 mg/kg, 40 mg/kg, or 80 mg/kg YDR1 orally, once daily for 3 days in C57BL/6 mice. Twenty-four hours after the last administration, mice were euthanized, plasma concentration of YDR1 was measured and spleen tissue was analyzed by Western blot for SMARCA2 expression. We observed a dose-dependent increase in plasma concentration of YDR1 ranging from about 100 nM in the 5 mg/kg group to 1.88 μM in the 80 mg/kg group (Figure 6a). Importantly, the dose-dependent degradation of SMARCA2 with the highest degradation of 70% was noted in the 80 mg/kg level (Figure 6b). While this was encouraging, it is below the level of degradation observed in human cancer cells *in vitro*. It is important to note that we have utilized pomalidomide as an E3 ligand recruiter in our PROTACs, and it is known that in mice, thalidomide and its analogs generally have a lower affinity to mouse cereblon due to the presence of isoleucine at position 391 in contrast to valine in humans. This has been demonstrated to result in steric clash and reduced affinity to mouse cereblon. This has inspired the development of genetically engineered mice harboring I391V substitution ($Crbn^{I391V}$) resulting in a better recapitulation of effect of thalidomide and analogs on human cells and tissues.[36,37] Hence, we next assessed the impact of our cereblon-dependent PROTAC YDR1 in $Crbn^{I391V}$ mice. Specifically, we administered vehicle control, 10, 20, 40, or 80 mg/kg YDR1 orally, once daily for 3 days in $Crbn^{I391V}$ mice. Twenty-four hours after the last administration, mice were euthanized, plasma concentration of YDR1 was measured and spleen tissue was analyzed by Western blot for SMARCA2 expression. We observed a dose-dependent increase in plasma concentration of YDR1 ranging from 1 μM in the 10 mg/kg group to 2.45 μM in the 80 mg/kg group (Figure 6c). Importantly, a more robust dose-dependent degradation of SMARCA2 with the highest degradation of 81% was noted in the 80 mg/kg dose (Figure 6d). At all doses tested, we see increased degradation of SMARCA2 (variance range of 11% to 38%) in $Crbn^{I391V}$ mice compared to C57BL/6 mice, indicating the usefulness of $Crbn^{I391V}$ mice for more accurate modeling of the effect of cereblon-based PROTACs. Importantly, we found that SMARCA4 was only modestly degraded by YDR1 compared to SMARCA2 in the spleens of both C57BL/6 and $Crbn^{I391V}$ mice, consistent with our in vitro selectivity data (Figure 6b,d; Figure S4b). Next, we sought to determine the ability of YDR1 to induce degradation of SMARCA2 in xenograft tumors. We implanted H1568 human lung cancer cells in the flanks of immunocompromised mice and performed YDR1 administration daily at 10 mg/kg, 20 mg/kg, 40 mg/kg, and 80 mg/kg for 4 days daily by oral gavage. Tumors were harvested, and SMARCA2 was probed by

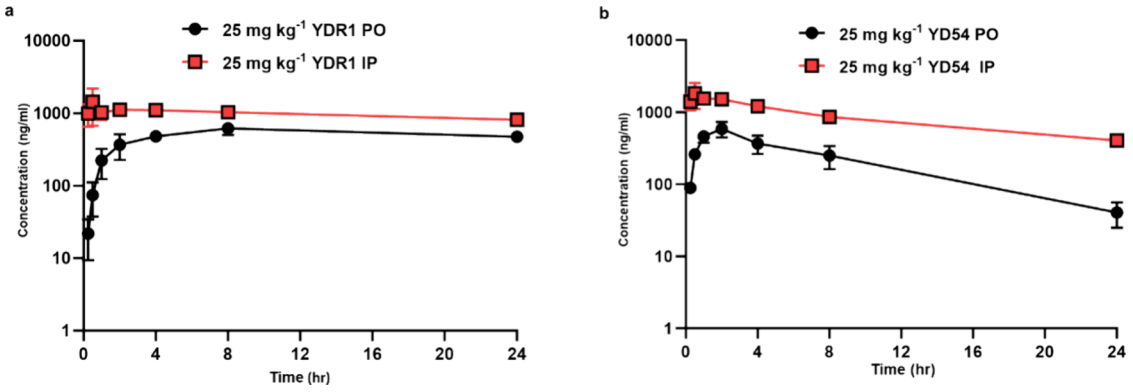

Figure 5. YDR1 and YD54 are orally bioavailable. Plasma concentrations of YDR1 and YD54 in male CD-1(ICR) mice following a single p.o and i.p dose over 24 h. (a) The amount of YDR1 in plasma was determined by LC-MS/MS. (b) The amount of YD54 in plasma was determined by LC-MS/MS. Values are shown as mean ± SEM (n = 3 mice for each time point).

https://doi.org/10.1021/acs.jmedchem.4c02577
J. Med. Chem. 2025, 68, 9202−9219

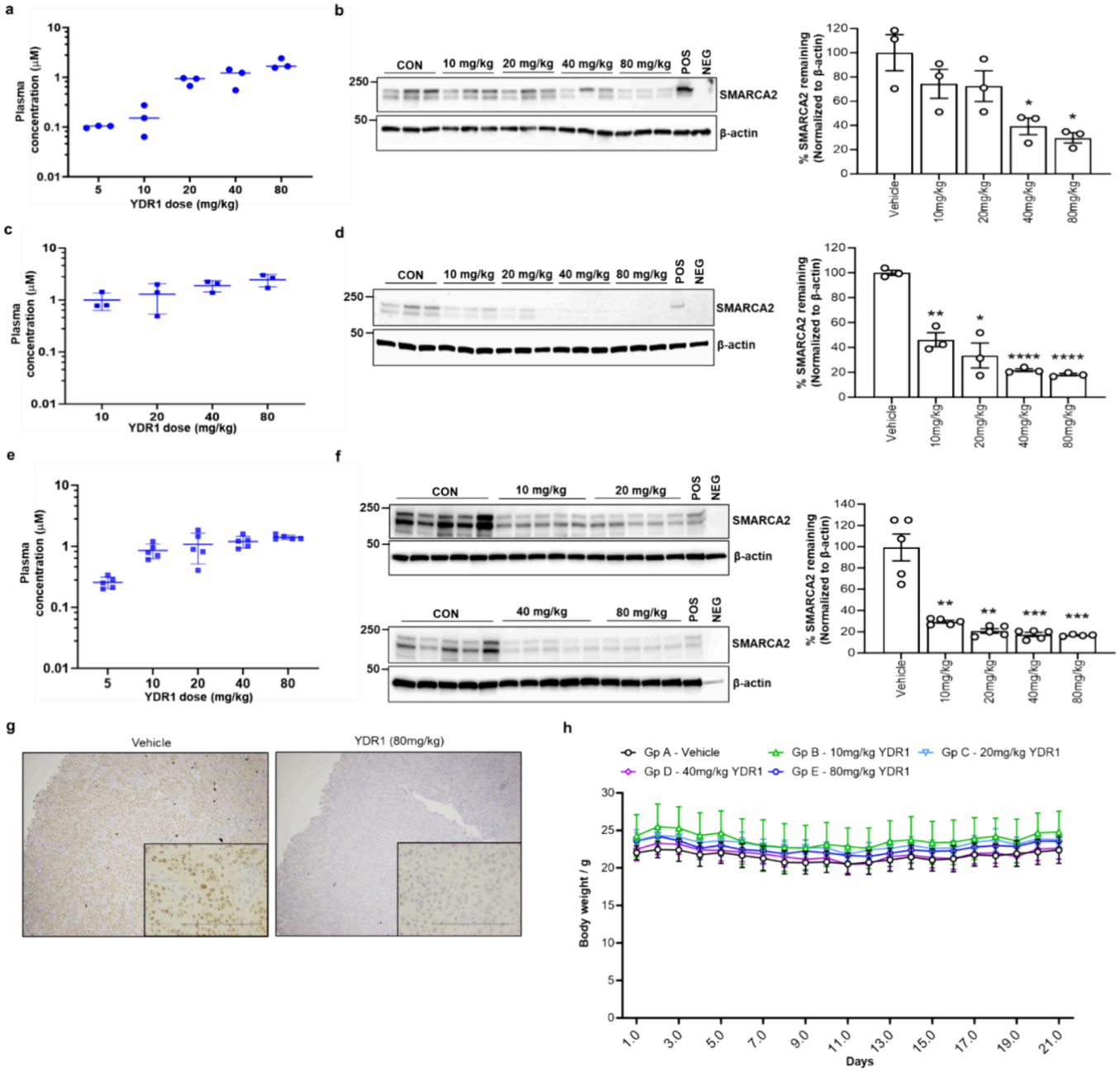

Figure 6. Pharmacokinetic and pharmacodynamic correlation studies of YDR1. Mice were treated with YDR1 by oral gavage at different doses for 3 days in C57BL/6 and *Crbn*$^{I391\ V}$ mouse model and 4 days in H1568 xenograft models. (a, d, e) Plasma concentrations of YDR1. (b, d, f) Target engagement of YDR1 on SMARCA2 protein levels in Spleen of C57BL/6 and *Crbn*$^{I391\ V}$ mouse, and tumors of H1568 Xenograft. Actin was used as the loading control. (g) Immunohistochemistry images of nuclear SMARCA2 in H1568 tumors. (h) Mouse body weight after treating each group with different doses of YDR1 for 21 days. Data is presented as mean ± SEM.

Western blot. YDR1 potently degraded SMARCA2 in this model with 87% degradation observed at 80 mg/kg (Figure 6e,f). We further validated this by robust reduction in SMARCA2 signal by immunohistochemical staining of tissue sections with SMARCA2 antibodies (Figure 6g). Lastly, we determined the medium-term tolerability of YDR1 by daily treatment of mice with increasing doses up to 80 mg/kg for 21 days. Overall, YDR1 was well tolerated in these mice, including at the highest dose, with minimal body weight loss and no obvious signs of toxicity or morbidity (Figure 6h).

Antitumor Activity of YDR1 and YD54 in *SMARCA4* Mutant Models of NSCLC. Having thus established the basic pharmacokinetics, tolerability, and target engagement of YDR1, we finally sought to determine its antitumor inhibitory activity using human xenograft tumor models. We first tested YDR1 in the H1568 xenograft model (*SMARCA4* mutant) in a female athymic nude and coadministered 40 mg/kg YDR1 once daily by oral gavage for 13 days. We found that YDR1 at 40m/kg moderately inhibited tumor growth with a tumor growth inhibition (TGI) of 27.6% compared to vehicle control (Figure 7a). YDR1 was well tolerated with no change in body weight (Figure 7b) and induced moderate degradation of SMARCA2 to about 50% (Figure 7c). As YD54 was generally more potent in cell-based assays, we wondered if YD54 could

https://doi.org/10.1021/acs.jmedchem.4c02577
J. Med. Chem. 2025, 68, 9202−9219

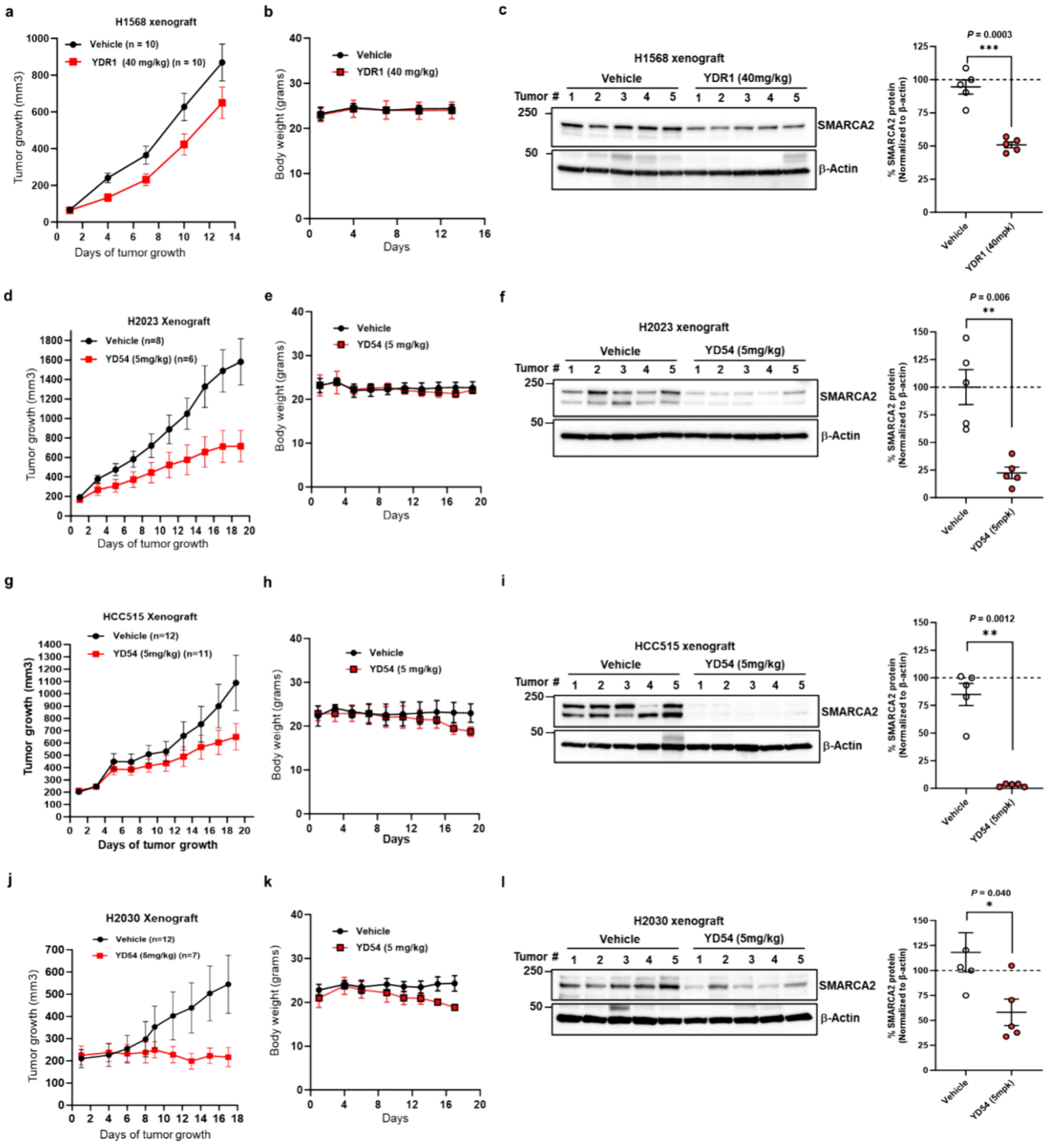

Figure 7. Antitumor efficacy of YDR1 and YD54 in *SMARCA4* mutant xenograft models of lung cancer. Mice were treated with YDR1 and YD54 by oral gavage daily for a given duration of days. (a, d, g, j) Average tumor volume for each dosing group. Data is presented as mean ± SEM (b, e, h, k) Mouse body weight in each group. Data is presented as mean ± SEM (c, f, i, l) Target engagement of YDR1 and YD54 on SMARCA2 protein levels in tumors of *SMARCA4* mutant lung xenografts. Tumors were collected after a 24 h time point after dosing for Western blotting analysis. *β*-Actin was used as the loading control.

have improved antitumor efficacy in vivo. Hence, we next tested YD54 in H2023, HCC515, and H2030 xenograft models (*SMARCA4* mutant) in female athymic nude and coadministered 5 mg/kg YD54 once daily by oral gavage for 19 days for both H2023 and HCC515 xenografts and 17 days of treatment in H2030 xenograft. We found that YD54 at 5 mg/kg inhibited tumor growth with a tumor growth inhibition (TGI) of 62.5, 48.8, and 93.4% in H2023, HCC515, and H2030 xenografts, respectively, compared to vehicle control (Figure 7d,g,j). In H1568 and H2023 xenografts antitumor efficacy experiments, YDR1 and YD54 caused no or minimal reduction in body weight (<10% compared to controls) and

https://doi.org/10.1021/acs.jmedchem.4c02577
J. Med. Chem. 2025, 68, 9202−9219

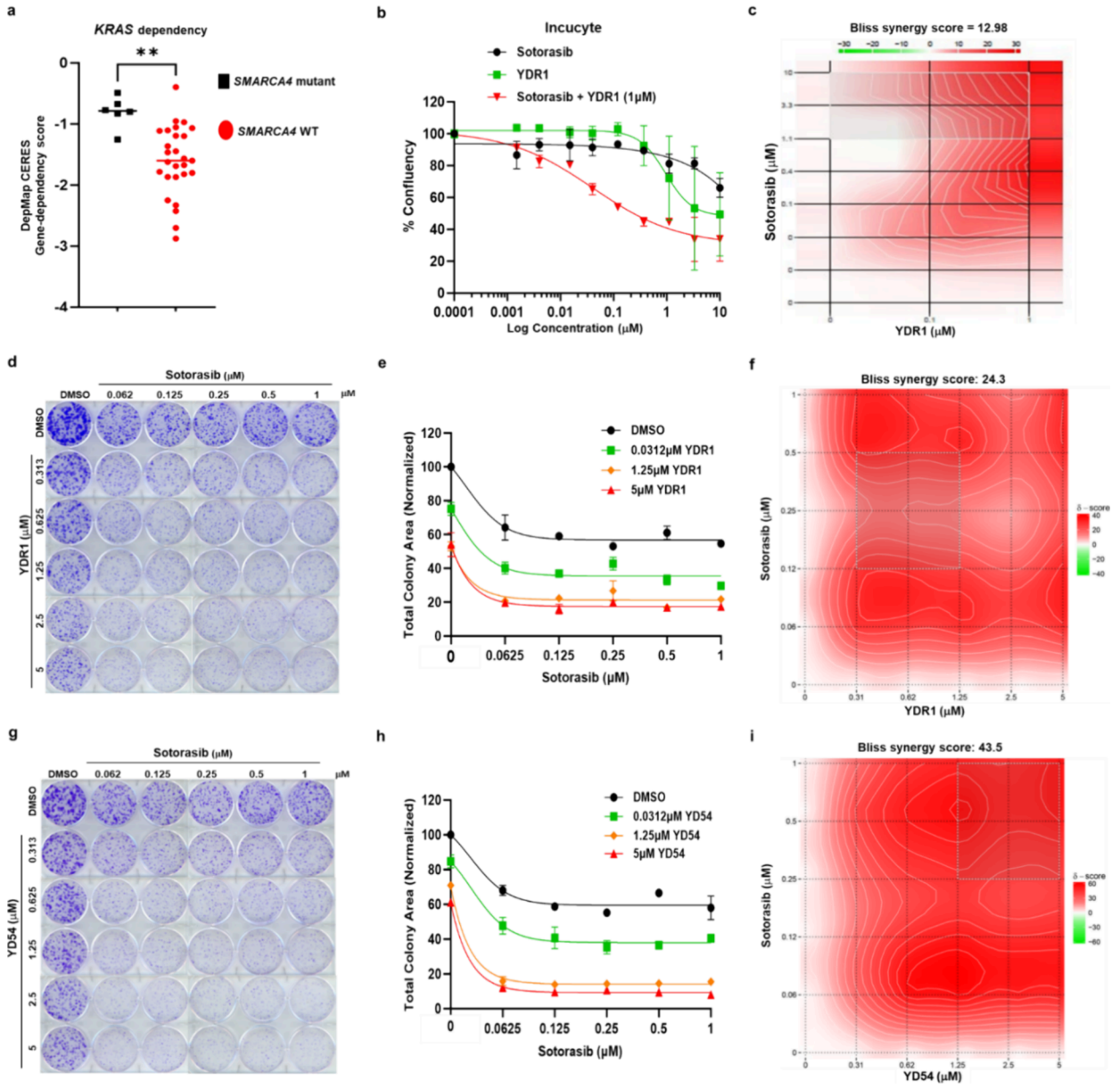

Figure 8. YDR1 and YD54 synergize with sotorasib to inhibit growth of sotorasib-resistant *KRAS*^{G12}and *SMARCA4* comutant cancer cells. (a) Graph shows *KRAS* dependency on *SMARCA4*-WT or *SMARCA4* mutant cell lines as revealed by CRISPR-Cas9 knockout screening data compiled from DepMap portal of the Broad Institute. (b) Incucyte-determined cell proliferation (% confluency) of H2030 cell line treated with sotorasib or YDR1 or combination. (c) Heatmaps of H2030 cell line treated as in (b) depict synergistic drug interactions using the Bliss independence model. d) Representative images of clonogenic growth assays in H2030 cells treated with sotorasib or YDR1 or combination. (e) Quantitation total colony area (normalized) in H2030 cell line treated as in (d). (f) Heatmaps of H2030 cell line depict synergistic drug interactions using the Bliss independence model. (g) Representative images of clonogenic growth assays in H2030 cell line treated with sotorasib or YD54 or in combination. (h) Quantitation total colony area (normalized) in H2030 cell line treated as in (g). (i) Heatmaps of H2030 cell line depict synergistic drug interactions using the Bliss independence model.

were tolerated at the doses and duration of the *in vivo* studies (Figure 7b,e). In HCC515 and H2030 xenograft antitumor efficacy experiments, YD54 caused minimal to moderate reduction in body weight (<20% compared to controls) potentially due to differences in formulation (1% Tween 80 compared to 0.2% Tween 80 in the above experiments) but otherwise YD54 was tolerated at the doses and duration of these *in vivo* studies (Figure 7h,k). Immunoblot analysis of individual tumor protein lysates from this study showed YD54 reduced SMARCA2 levels by 76, 96, and 40% compared to vehicle control-treated tumors (Figure 7f,i,l).

YDR1 and YD54 Synergize with Sotorasib to Inhibit Growth of Sotorasib-Resistant *KRAS*^{G12C} and *SMARCA4* Comutant Cancer Cells. It is worth noting that YDR1 and YD54 did not induce tumor regression in any of our experiments, which is consistent with other antitumor efficacy studies employing other SMARCA2 PROTACs,[23,24] suggesting that the identification of synergistic combinations is required for efficient clinical translation. Importantly, a recent clinical report showed that comutations in tumor suppressors (*SMARCA4, KEAP1, and CDKN2A*) predict poorer response to KRAS^{G12C} inhibitors in lung cancer patients.[38] This study

https://doi.org/10.1021/acs.jmedchem.4c02577
J. Med. Chem. 2025, 68, 9202−9219

identified both inferior overall survival (OS) and progression-free survival (PFS) among patients with *SMARCA4* mutation (PFS: 1.6 vs 5.4 months, OS: 4.9 vs 11.8 months, for mutant vs WT *SMARCA4*). Interestingly, an elegant study of *KRAS* mutant rhabdoid tumors with concomitant loss of *SMARCB1* (*another key SWI/SNF subunit*) showed a lack of activation of the MAPK signaling pathway, indicating that SWI/SNF inactivation can lead to "partial independence" from the upstream RAS pathway.[39] We initially corroborated the clinical data that suggested that *SMARCA4* mutant tumors have a poor response to $KRAS^{G12C}$ inhibitors by analyzing the vast functional genomics data from the DepMap Project[40] that assessed the dependency of lung cancer cell lines for growth and survival on *KRAS*. We categorized *KRAS* mutant lung cancer cell lines by *SMARCA4* status and asked if there was a difference in genetic dependency on *KRAS*. We showed that indeed *SMARCA4* and $KRAS^{G12C}$ comutant cell lines are significantly less dependent on *KRAS* than *SMARCA4* WT cells (Figure 8a). Hence, we hypothesized that the cotreatment of tumors harboring both $KRAS^{G12C}$ and *SMARCA4* mutations with the combination of SMARCA2 PROTAC and $KRAS^{G12C}$ inhibitor might have a synergistic effect. We used the H2030 cell line, which harbors $KRAS^{G12C}$ mutation and *SMARCA4* deletion, for our investigations. We treated these cells with 3-fold diluted concentrations of sotorasib or YDR1 or a combination of both and performed a 7 day cell growth measured by incucyte. While we observed minimal growth inhibition by the single agents, the combination induced a robust synergistic growth inhibition (Figure 8b). We next confirmed the statistical significance of growth inhibition by the combination of YDR1 and Sotorasib by estimating the Bliss/Lowe consensus synergy score (>10 indicates synergy) from SynergyFinder[41] (Figure 8c). We corroborated this by performing 8 day clonogenic assays, which similarly showed robust and significant synergy when H2030 cells were treated with 2-fold diluted concentrations of sotorasib or YD54 or a combination of both (Figure 8d–f). We further corroborated these findings by performing clonogenic assays with H2030 cells treated with 2-fold diluted concentrations of sotorasib or YD54 or a combination of both. We confirmed the statistical significance of growth inhibition by the combination of YD54 and sotorasib by estimating the Bliss/Lowe consensus synergy score (>10 indicates synergy). We observed more synergistic effects of the combination of YD54 and sotorasib than the combination of YDR1 and sotorasib (Figure 8g–i) in line with the higher potency of YD54. Finally, we sought to probe whether the addition of SMARCA2 degraders has any impact on the MAPK signaling pathway, which is a key downstream target of KRAS inhibitors. To this end, Western blots were done on cells that were treated with vehicle, sotorasib, YDR1, YD54, or a combination of sotorasib and YDR1 or sotorasib and YD54. While sotorasib robustly reduced phosphorylation of ERK, the addition of either YDR1 or YD54 further reduced this phosphorylation level (Figure S5a,b).

The demonstration of the synergistic combination effect of YDR1 or YD54 with sotorasib in a sotorasib-resistant H2030 cell line is highly promising and could enable expansion of the therapeutic indications for both SMARCA2 PROTACs and $KRAS^{G12C}$ inhibitors. Taken together, YDR1 and YD54 were identified as novel SMARCA2 PROTACs that selectively degrade SMARCA2, allowing for an efficacious antitumor effect as a single agent or in combination with $KRAS^{G12C}$ inhibitors in *SMARCA4* mutant cancer.

DISCUSSION AND CONCLUSIONS

Targeted protein degradation is a rapidly evolving therapeutic modality with substantial potential in cancer treatment. Human and mouse genetics as well as pharmacologic evidence have firmly established that *SMARCA2* is synthetic lethal to *SMARCA4,* required for growth and survival of *SMARCA4* mutant cancer cells, and a highly desirable therapeutic target.[16,17,19,20,23,24] The strength of the genetic interaction, coupled with the large number of patients harboring *SMARCA4* mutations across multiple cancer types, strongly suggests that therapeutics targeting this synthetic lethality could have paradigm-shifting consequences like PARP inhibitors in *BRCA* mutant tumors. Hence, there is intense effort to develop SMARCA2 inhibitors and take advantage of this vulnerability of *SMARCA4* mutant cancers. So far, the major challenge has been the fact that the readily ligand-accessible SMARCA2 bromodomain is not required for this synthetic lethal interaction;[16] hence, mere inhibition of the bromodomain has no therapeutic utility. Since potent SMARCA2 bromodomain ligands exist,[30] PROTACs provide a unique opportunity to utilize these bromodomain ligands as hooks and enable the degradation of the entire protein to achieve therapeutic utility. To date, multiple potent SMARCA2 PROTACs have been reported.[17,23−25] Importantly, these PROTACs have utilized the VHL E3 ubiquitin ligase and shown promising antitumor activities. Since one of the major mechanisms of cancer resistance to PROTACs is genomic alterations in the E3 ligase targeted by the PROTAC, it is highly desirable to have a toolbox of PROTACs with nonoverlapping E3 ligases.[28]

To expand the repertoire of SMARCA2 PROTACs using alternative E3 ligases, we report the discovery of YD54 and YDR1, two potent and selective SMARCA2-degrading PROTACs based on the E3 ligase cereblon. Optimization of linkers, aptly named linkerology, is a key factor in PROTAC design,[42,43] and in our studies, rigid heterocyclic ring-containing linkers were found to improve potency, metabolic stability, and pharmacokinetic properties of PROTACs. We performed in-depth biochemical, cellular, and pharmacologic characterization of these compounds and showed that they have highly selective growth inhibitory activity against *SMARCA4* mutant cancer cells (100 to 800-fold).

Selective SMARCA2 degraders (with limited activity against SMARCA4) are desirable for clinical development due to the anticipated toxicities of unintended SMARCA4 degradation. This is borne out of mouse knockout studies that showed essentiality of SMARCA4 for tissue maintenance as well as overt toxicity in mice by pharmacologic inhibitors of SMARCA4 ATPase activity.[21,44,45] YDR1 and YD54 show enhanced selectivity for SMARCA2 over SMARCA4 by immunoblotting. Mechanistically, consistent with our published results, YDR1 and YD54 increased phosphorylation of S127 and S109 residues of YAP1 in *SMARCA4* mutant cells, likely inactivating YAP's activity. Furthermore, at the global level, quantitative proteomics showed that SMARCA2 is the most significantly degraded protein among 8626 proteins analyzed, while SMARCA4 was not. YDR1 was also well tolerated in mice up to 21 days of treatment, suggesting the existence of a likely therapeutic window. Importantly, we showed that YDR1 and YD54 were orally bioavailable and showed potent SMARCA2 degradation profiles in mouse tissues as well as in implanted xenograft tumors. Lastly, we

https://doi.org/10.1021/acs.jmedchem.4c02577
J. Med. Chem. 2025, 68, 9202−9219

demonstrated robust antitumor growth inhibition in *SMARCA4* mutant xenograft models of lung cancer.

Finally, we were inspired by a recent clinical observation that showed that comutations in tumor suppressors such as *SMARCA4* predict poorer response to $KRAS^{G12C}$ inhibitors in lung cancer patients[38] to conduct combination studies. We were able to test and confirm our hypothesis that the cotreatment of tumors harboring both $KRAS^{G12C}$ and *SMARCA4* mutation with the combination of SMARCA2 PROTAC and $KRAS^{G12C}$ inhibitor has a synergistic growth inhibitory effect. Our demonstration of the synergistic combination effect of YDR1 or YD54 with Sotorasib in a sotorasib-resistant H2030 cell line is highly promising and could enable expansion of the therapeutic indications of SMARCA2 PROTACs and $KRAS^{G12C}$ inhibitors.

As orally bioavailable compounds, our PROTACs are an improvement on intravenously administered agents. Despite their promising potency, selectivity and PK profiles, our PROTACs have some limitations that we describe here. While YDR1 and YD54 show preferential selectivity to SMARCA2 over SMARCA4, at higher doses, they also induce degradation of SMARCA4, which can result in unintended adverse effects and needs to be carefully studied. Further, our PROTACs are less potent than the recently reported ACBI2, a VHL-based degrader that has a faster onset of action. Importantly, our PROTACs did not induce tumor regression but only growth inhibition. This could be due to rapid rewiring of the chromatin and epigenetic landscape providing cancer cells escape mechanisms. While data is still evolving, lack of tumor regression across most model systems appears to be a common theme of SMARCA2 PROTACs, suggesting identification of synergistic combination partners is paramount for successful clinical development. Thus, future efforts toward identification of the genetic determinants of response and resistance coupled to systematic studies into combination partners are needed.

In summary, we discovered a novel series of SMARCA2 PROTACs based on cereblon E3 ligase harboring rigid heterocyclic ring-based linkers. Quantitative proteomics showed these compounds showed enhanced selectivity for degrading SMARCA2 over SMARCA4. Further, in vitro growth assays showed profound selectivity of YD series SMARCA2 PROTACs for *SMARCA4* mutant cancer cells. Importantly, YDR1 was orally bioavailable and well-tolerated in mice. Additionally, YDR1 and YD54 were shown to have potent SMARCA2 degrading activity in mouse tissue and xenograft tumors with robust tumor growth inhibitory activity in *SMARCA4* mutant xenograft tumors. Finally, we demonstrated the synergistic combination effect of YDR1 with sotorasib against a sotorasib-resistant $KRAS^{G12C}$ and *SMARCA4* comutant cell line for the first time. We anticipate that this study will stimulate future preclinical and clinical investigations to target *SMARCA4* mutant cancers and expand the translational potential of SMARCA2 degraders as single or combination agents in the appropriate genomically defined subtypes of lung cancer.

Experimental Section. *Materials and Methods. Chemical Synthesis of YDR1 and YD54.* All commercial chemical reagents and solvents were used directly without additional purification unless specifically indicated. Liquid chromatography mass spectra (LCMS) were recorded on SHIMADZU LCMS-2020, and high-performance liquid chromatography (HPLC) was recorded on SHIMADZU LC-20AB. Proton nuclear magnetic resonance (^{1}H NMR) spectra and (^{19}F NMR) spectra were recorded on a Bruker 400 MHz instrument. Chemical shifts were reported in parts per million (ppm), and the residual solvent peak was used as an internal reference: proton (chloroform δ 7.27, DMSO δ 2.50, CH3OH δ 3.34). The NMR data was expressed in the following format: (d) chemical shift (multiplicity, J values in Hz, integration). The abbreviations used are as follows: s = singlet, d = doublet, t = triplet, q = quartet, m = multiplet. Most compounds were purified by column chromatography (SiO2). The purity of the final compound was analyzed by HPLC analysis (SHIMADZU LC-20AB; XBridge C18, 2.1 × 50 mm, 5 μm; 10%−80% MeCN in H2O containing 0.025% NH3·H2O in 6 min; 0.8 mL/min). Synthesis and characterization of YDR1, YD54, and related compounds are detailed below. NMR spectra for compounds YDR1 and YD54 and HPLC spectra for YDR1 and YD54 are provided (Supplemental Data 1 and 2). All compounds are confirmed to be >95% pure by HPLC.

Synthetic Scheme for YDR1. Preparation of YDR1. To a solution of compound **1** (4.00 g, 16.0 mmol, 1.00 equiv) in DMSO (40.0 mL) was added IBX (6.74 g, 24.1 mmol, 1.50 equiv). The mixture was stirred at 15 °C for 2 h. LCMS (EW28004−8-P1A2) showed that compound **1** was consumed completely, and one main peak with the desired mass was detected. The mixture was diluted with H_2O (100 mL) and extracted with EtOAc (100 mL × 2). The combined organic layers were washed with brine (100 mL), dried over Na_2SO_4, filtered, and concentrated under reduced pressure to give a residue to afford the crude compound **2** (3.70 g, crude) as a colorless oil and was used in the next step without further purification.

LCMS: EW28004−8-P1B, R_t = 0. 993 min, m/z = 464.2 (M + 1).

^{1}H NMR: EW28004−8-P1A (400 MHz, $CDCl_3$).

δ 9.67 (s, H), 7.39−7.31 (m, 5H), 5.14 (s, 2H), 4.08−4.05 (m, 2H), 3.07−3.01 (m, 2H), 2.48−2.41 (m, 1H), 1.91 (m, 2H), 1.64−1.54 (m, 2H). To a solution of compound **2** (3.70 g, 14.9 mmol, 1.00 equiv) and *tert*-butyl piperazine-1-carboxylate (2.93 g, 15.7 mmol, 1.05 equiv) in (40.0 mL) was added HOAc (898 mg, 14.9 mmol, 856 μL, 1.00 equiv) and $NaBH(OAc)_3$ (4.76 g, 22.4 mmol, 1.50 equiv). The mixture was stirred at 15 °C for 12 h. LCMS (EW28004−9-P1A) showed that compound **2** was consumed completely, and one main peak with the desired mass was detected. The mixture was diluted with H_2O (100 mL) and extracted with DCM (100 mL × 2). The combined organic layers were washed with brine (100 mL), dried over Na_2SO_4, filtered, and concentrated under reduced pressure to give a residue to afford compound **3** (6.00 g, crude) as a white solid.

LCMS: EW28004−9-P1B, R_t = 0.798 min, m/z = 418.2 (M + 1).

^{1}H NMR: EW28004−9-P1A (400 MHz, $CDCl_3$).

δ 7.39−7.30 (m, 5H), 5.13 (s, 2H), 4.18 (s, 2H), 3.41 (d, J = 4.8 Hz, 4H), 2.77 (m, 2H), 2.34 (d, J = 4.8 Hz, 4H), 2.17 (t, J = 7.2 Hz, 2H), 1.77−1.74 (m, 2H), 1.46 (s, 9H), 1.27 (m, 1H), 1.17−1.07 (m, 2H). To a solution of compound **3** (4.00 g, 9.58 mmol, 1.00 equiv) in MeOH (40.0 mL) was added Pd/C (0.40 g, 958 μmol, 10.0% purity, 0.10 equiv) under N_2. The suspension was degassed under vacuum and purged with H_2 several times. The mixture was stirred under H_2 (15 psi) at 15 °C for 2 h. TLC (petroleum ether: ethyl acetate = 1:1) showed that reactant **1** was consumed completely, and one major new spot with larger polarity was detected. The mixture was filtered and the filtered cake was washed with MeOH (100 mL),

https://doi.org/10.1021/acs.jmedchem.4c02577
J. Med. Chem. 2025, 68, 9202−9219

concentrated under reduced pressure to afford compound **4** (2.20 g, crude) as a gray solid.

^{1}H NMR: EW28004−10-P1A (400 MHz, $CDCl_3$).

δ 3.41 (d, J = 4.8 Hz, 4H), 3.10−3.07 (m, 2H), 2.63−2.51(m, 2H), 2.33 (d, J = 4.8 Hz, 4H), 2.16 (t, J = 7.2 Hz, 2H), 2.05 (s, 1H), 1.75−1.72 (m, 2H), 1.65−1.58 (m, 1H), 1.46 (s, 9H), 1.15−1.05 (m, 2H).

To a solution of compound **4** (2.20 g, 7.76 mmol, 1.00 equiv) and 3,4-difluorobenzaldehyde (1.16 g, 8.15 mmol, 884 μL, 1.05 equiv) in DMF (20.0 mL) was added Et_3N (1.18 g, 11.6 mmol, 1.62 mL, 1.50 equiv). The mixture was stirred at 90 °C for 4 h. LCMS (EW28004−11-P1A) showed compound **4A** was consumed completely, and one main peak with the desired mass was detected. The mixture was diluted with H_2O (100 mL) and extracted with EtOAc (50 mL × 2). The combined organic layers were washed with brine (30 mL× 2), dried over Na_2SO_4, filtered, and concentrated under reduced pressure to give a residue. The residue was purified by column chromatography (SiO_2, Petroleum ether/Ethyl acetate = 10/1 to 1/1, R_f = 0.40) to afford compound **5** (2.30 g, 4.82 mmol, 62.0% yield, 84.9% purity) as a yellow solid.

LCMS: EW28004−11-P1B, R_t = 0.799 min, m/z = 406.2 (M + 1).

HPLC: EW28004−11-P1B1, R_t = 1.535 min.

^{1}H NMR: EW28004−11-P1A (400 MHz, $CDCl_3$).

δ 9.81−9.80 (m, 1H), 7.56−7.48 (m, 2H), 6.99−6.96 (m, 1H), 3.70−3.67 (m, 2H), 3.43 (m, 4H), 2.85−2.79 (m, 2H), 2.36 (m, 4H), 2.23 (t, J = 7.2 Hz, 2H), 1.88 (t, J = 12.4 Hz, 2H), 1.74−1.68 (m, 1H), 1.47 (s, 9H), 1.40−1.36 (m, 2H). To a solution of compound **5** (1.00 g, 2.47 mmol, 1.00 equiv) and 2-(6-amino-5-(piperazin-1-yl)pyridazin-3-yl)phenol hydrochloride (704 mg, 2.59 mmol, 1.05 equiv) in DMSO (10.0 mL) was added $NaBH(OAc)_3$ (1.05 g, 4.94 mmol, 2.00 equiv). The mixture was stirred at 15 °C for 12 h. LCMS (EW28004−12-P1A) showed that compound **5** was consumed completely, and one main peak with the desired mass was detected. The mixture was diluted with H_2O (30 mL) and extracted with EtOAc (50 mL × 2). The combined organic layers were washed with brine (30 mL× 2), dried over Na_2SO_4, filtered, and concentrated under reduced pressure to give a residue. The crude product was triturated with PE (10.0 mL) for 15 min. Then the mixture was filtered, and the filtered cake was washed with Petroleum ether (3 mL × 2) to afford compound **6** (1.00 g, 1.37 mmol, 55.3% yield, 90.3% purity) as a yellow solid.

LCMS: EW28004−12-P1B, R_t = 0.741 min, m/z = 661.3 (M + 1).

^{1}H NMR: EW28004−12-P1A (400 MHz, $CDCl_3$).

δ 13.7 (s, 1H), 7.59−7.57 (m, 1H), 7.32−7.28 (m, 2H), 7.06−7.00 (m, 3H), 6.94−6.89 (m, 2H), 4.85 (s, 2H), 3.54 (s, 2H), 3.45 (m, 6H), 3.17 (s, 3H), 2.69−2.64 (m, 6H), 2.40 (s, 4H), 2.28−2.26 (m, 2H), 1.89−1.87 (m, 2H), 1.66 (m, 1H), 1.47 (s, 9H), 1.40−1.36 (m, 2H).

A solution of compound **6** (500 mg, 756 μmol, 1.00 equiv) in HCl/EtOAc (5.00 mL) was stirred at 15 °C for 2 h. LCMS (EW28004−13-P1A) showed that compound **6** was consumed completely, and one main peak with the desired mass was detected. The mixture was concentrated under reduced pressure to give a residue to afford compound **7** (400 mg, crude, HCl) as a yellow solid.

LCMS: EW28004−13-P1B, R_t = 0.711 min, m/z = 561.3 (M + 1).

^{1}H NMR: EW28004−13-P1A (400 MHz, $CDCl_3$).

δ 12.7 (s, 1H), 10.2 (s, 2H), 7.59−7.57 (m, 1H), 7.32−7.28 (m, 2H), 7.06−7.00 (m, 3H), 6.94−6.89 (m, 2H), 4.85 (s, 2H), 3.54 (s, 2H), 3.45 (m, 6H), 3.17 (s, 3H), 2.69−2.64 (m, 6H), 2.40 (s, 4H), 2.28−2.26 (m, 2H), 1.89−1.87 (m, 2H), 1.66 (m, 1H), 1.40−1.36 (m, 2H). To a solution of compound **7** (200 mg, 335 μmol, 1.00 equiv, HCl) and 2-(2,6-dioxopiperidin-3-yl)-5-fluoroisoindoline-1,3-dione (97.1 mg, 352 μmol, 1.05 equiv) in DMF (2.00 mL) was added DIEA (216 mg, 1.67 mmol, 292 μL, 5.00 equiv). The mixture was stirred at 90 °C for 12 h. LCMS (EW28004−14-P1A3) showed that compound **7** was consumed completely, and one main peak with the desired mass was detected. The mixture was diluted with H_2O (20.0 mL) and extracted with ethyl acetate (20.0 mL × 2). The combined organic layers were washed with brine (10.0 mL × 2), dried over Na_2SO_4, filtered, and concentrated under reduced pressure to give a residue. The residue was purified by Prep-HPLC (column: Waters Xbridge C18 150*50 mm* 10um; mobile phase: [water(10 mM NH4HCO3)-ACN]; B%: 48−78%,11 min) to afford **YDR1** (50.0 mg, 59.5 μmol, 17.8% yield, 97.3% purity) as a yellow solid.

LCMS: EW28004−14-P1C1, R_t = 1.061 min, m/z = 817.0 (M + 1).

HPLC: EW28004−14-P1C2, R_t = 2.611 min.

^{1}H NMR: EW28004−14-P1A (400 MHz, $CDCl_3$).

FNMR: EW28004−14-P1A.

δ 13.7 (s, 1H), 8.20 (s, 1H), 7.70 (t, J = 8.4 Hz, 2H), 7.60−7.58 (m, 1H), 7.33 (s, 2H), 7.31−7.29 (m, 2H), 4.97−4.93 (m, 1H), 4.82 (s, 2H), 3.55 (s, 2H), 3.46−3.40 (m, 6H), 3.18 (s, 4H), 2.92−2.77 (m, 3H), 2.74−2.72 (m, 1H), 2.71−2.66 (m, 5H), 2.61 (s, 4H), 2.33 (t, J = 6.8 Hz, 2H), 2.18−2.09 (m, 1H), 1.89 (t, J = 12.4 Hz, 2H), 1.53−1.40 (m, 3H).

Preparation of YD54. To a solution of cpd **1** (1.00 g, 7.04 mmol, 763 μL) in CH_3CN (20.0 mL) was added Et_3N (1.42 g, 14.0 mmol, 1.96 mL) and *tert*-butyl piperazine-1-carboxylate (1.57 g, 8.44 mmol). The mixture was stirred at 80 °C for 10 h. TLC (Petroleum ether: Ethyl acetate = 5:1) showed that some of the starting material remained and a main spot (Rf = 0.25) was formed. The reaction mixture was filtered, and the filter liquor was concentrated to give the crude product. The residue was purified by column chromatography (SiO_2, Petroleum ether/Ethyl acetate = 30/1 to 5/1) to give cpd **2** (0.80 g, 2.59 mmol, 36.8% yield) as light-yellow oil.

LCMS: EW16633−201-P1B1, R_t = 0.963 min, m/z = 253.1 $(M + H)^+$.

To a solution of cpd **2** (1.00 g, 3.24 mmol) in DMSO (10.0 mL) was added 2-(6-amino-5-piperazin-1-yl-pyridazin-3-yl) phenol (967 mg, 3.57 mmol, HCl salt), $NaBH(OAc)_3$ (824 mg, 3.89 mmol) and Et_3N (656 mg, 6.49 mmol, 902 μL). The mixture was stirred at 20 °C for 12 h. TLC (Petroleum ether: Ethyl acetate = 1:1, P1:Rf = 0.25) showed the start material remained and some new spots were detected. The reaction mixture was diluted with H_2O (30 mL) and then extracted with DCM (20 mL × 2). The combined organic layers were washed with brine (10 mL × 2), dried over Na_2SO_4, filtered, and concentrated under reduced pressure to give a residue. The residue was purified by column chromatography (SiO2, Petroleum ether/Ethyl acetate = 10/1 to 2/1) to afford cpd **3** (450 mg, 784 μmol, 24.2% yield, 98.3% purity) as a white solid.

LCMS: EW20934−239-P1B3, R_t = 0.805 min, m/z = 564.4 $(M + H)^+$.

https://doi.org/10.1021/acs.jmedchem.4c02577
J. Med. Chem. 2025, 68, 9202−9219

To a solution of cpd **3** (400 mg, 709 μmol) in MeOH (4.00 mL) was added HCl/MeOH (4 M, 4.00 mL). Then, the mixture was stirred at 20 °C for 1 h. The mixture was concentrated under reduced pressure to give a residue. The mixture was suspended in DCM (10 mL), and then the pH was adjusted to 8−9 with saturated NaHCO3 solution. Then, the mixture was extracted with DCM (20.0 mL × 2). The combined organic layers were washed with brine (10 mL), dried over Na_2SO_4, filtered, and concentrated under reduced pressure to afford cpd **4** (300 mg, 628 μmol, 88.5% yield, 97.1% purity) as a white solid.

LCMS: EW20934−242-P1A3, R_t = 1.033 min, m/z = 464.1 $(M + H)^+$.

^{1}H NMR: EW20934−242-P1A, (400 MHz, DMSO-d_6).

δ 14.4−14.2 (m, 1H), 8.0−7.9 (m, 1H), 7.51 (s, 1H), 7.30−7.21 (m, 1H), 7.09−7.03 (m, 2H), 7.01−6.95 (m, 1H), 6.95−6.82 (m, 2H), 6.24 (s, 2H), 3.49 (s, 2H), 3.11 (s, 4H), 3.02−2.98 (m, 8H), 2.58 (s, 5H).

To a solution of cpd **4** (203 mg, 431 μmol) in DMF (2.00 mL) was added cpd **5** (200 mg, 431 μmol) and Et_3N (43.6 mg, 431 μmol, 60.0 μL). The mixture was stirred at 20 °C for 2 h. The mixture was purified by Prep-HPLC (neutral condition) to give **YD54** (15.0 mg, 18.0 μmol, 4.18% yield, 91.8% purity) as a white solid.

LCMS: EW28074−31-P1A1, R_t = 0.702 min, m/z = 764.3 $(M + H)^+$.

HPLC: EW28074−31-P1A2, R_t = 1.160 min, purity = 95.9%.

^{1}H NMR: EW28074−31-P1A (400 MHz, $CDCl_3$).

δ 14.1−13.4 (m, 1H), 8.42−8.39 (m, 1H), 7.88−7.76 (m, 1H), 7.58−7.46 (m, 1H), 7.48 (m, 1H), 7.32−7.30 (m, 1H), 7.28−7.27 (m, 1H), 7.25−7.22 (m, 1H), 7.18−7.08 (m, 3H), 7.06−6.89 (m, 2H), 4.98−4.94 (m, 1H), 4.82 (s, 2H), 4.42 (s, 2H), 3.54 (s, 2H), 3.25−3.18 (m, 8H), 3.06−3.01 (m, 2H), 2.94−2.76 (m, 7H), 2.73−2.55 (m, 4H), 2.17−2.08 (m, 1H).

F NMR: EW28074−31-P1A (400 MHz, $CDCl_3$).

SFC: EW28074−31-P1A_c1424, Rt= 0.555 min.

Cell Culture. H1792, H322, HCC44, H2122, H1693, H1568, H2023, HCC515 and H2030 cell lines were cultured in RPMI (Roswell Park Memorial Institute 1640 Medium, Hyclone, Cat# SH30027.01; no pyruvate) with 10% heat inactivated fetal bovine serum (Gibco, Cat# 1614007), 1% penicillin/streptomycin (Hyclone, Cat# SV30010), and 2 mM L-glutamine. Cell lines were cultured until 80% confluency, kept at low passage numbers and maintained at 37 °C in a humidified 5% CO2-containing incubator. H1792, H2122, H1693, H1568, H2023, and H2030 cells were obtained from ATCC. HCC515 cell line were obtained from University of Texas Southwestern Medical Centre. H322 cell line was obtained obtained from Sigma. HCC44 was obtained from Leibniz Institute DSMZ. Routine Mycoplasma testing was performed using a Mycoplasma Detection Kit (ABM, Cat # G238). STR profiling for cell lines was done at MD Anderson Cancer Center core facility.

Compounds and Antibodies. Bortezomib (Cat# 10008822) was purchased from Cayman Chemical Company. Methylcellulose (Cat# M0262) was purchased from Millipore Sigma. Sotorasib (Cat# HY-114277) and pevonedistat (Cat# HY-70062) were purchased from MedChemExpress (South Brunswick Township, NJ). Pomalidomide (Cat# S1567) was purchased from Selleck Chemicals. Antibodies against SMARCA2 (Cat# 11966, 1:1000), SMARCA4 (Cat# 49360), YAP1 (Cat# 14074), Ser127YAP1 (Cat# 13008), Ser109YAP1 (Cat# 53749), ERK (Cat# 9102), and pERK (Cat# 4370) were from Cell Signaling (Danvers, MA, USA). β-Actin (Cat #A2228, 1:20,000) was from Millipore Sigma (Burlington, MA). DMSO was from Fisher Scientific (Cat# BP231−100). Sodium chloride and Tween 80 were from Sigma-Aldrich (Cat# 4780).

Cell Proliferation and Colony Formation Assays. Single-cell suspensions of all cell lines were counted and plated into 6-well plates at a density of 0.5−2 × 10^3 cells per well. Cells were cultured in a medium containing the indicated drugs for 9−14 days (refreshed every fifth day). At the endpoints, cells were fixed with formalin (10%), stained with crystal violet (0.01%w/v in water), and scanned. The total colony area was calculated with a Gelcount (Optronix) instrument. All experiments were performed in triplicate. IncuCyte S3 (Essen Biosciences, Ann Arbor, MI, USA) was used to measure cell proliferation. For IncuCyte S3 experiments, H2030 cells were suspended in fresh growth media, plated in 96-well plates at 500 cells/well, and grown overnight at 37 °C. On the following day, cells were treated with the drug, and confluency was assessed every 4 h until the end of the experiment. Confluency was determined at each time point using the IncuCyte S3 analysis software.

Immunohistochemistry. Xenograft lung tumors were fixed in formalin for 24 h, paraffin-embedded, sectioned, and stained according to standard procedures. After antigen retrieval in citrate buffer (pH: 6), slides were immersed in 3% hydrogen peroxide for 10 min. Nonspecific signals were blocked for 1 h using 2.5% normal goat serum. Slides were stained using respective antibodies overnight at 4 °C, SMARCA2 (Cat#11966, Cel Signaling 1:2000). Slides were washed and incubated with ImmPRESS-HRP conjugated antimouse or antirabbit cocktail from Vector Laboratories (MP-7451 and MP-7452) for 30 min at room temperature. The slides were thrice washed and stained with DAB substrate (VECTOR, SK-4105). The slides were counterstained with hematoxylin for 1 min and mounted with a mounting medium. After DAB staining, slides were dehydrated thrice in ethanol and thrice in xylene (1 min each) and mounted using Cytoseal 60. Images were further taken with the Vectra 3 automated quantitative pathology imaging system. Five images were acquired for each tumor, and images were processed using the Inform 2.5 software from Akoya Biosciences. Images were prepared based on a spectral library that detects DAB and Hematoxylin.

Immunoblotting. Cells were washed in ice-cold PBS, and proteins were extracted in RIPA buffer having protease and phosphatase inhibitors for 30 min. Lysates were then collected and centrifuged at 14,000 rpm for 15 min at 4 °C. Protein concentrations were measured using the BCA Protein Assay Kit (Thermo Scientific). Lysates were mixed with freshly made 4× Laemmli buffer, boiled at 95 °C for 10 min, and processed with mini-protean gel electrophoresis systems (Bio-Rad) using Bis-Tris 4−20% gradient precast gels (Biorad).

Calculation of DC_{50} and D_{max}. The protein expression of SMARCA2, SMARCA4, and β-actin was determined from Western blots, and ImageJ software was used for quantification. SMARCA2 and SMARCA4 expression was normalized to β-actin. The expression level of SMARCA2 and SMARCA4 in DMSO-treated cells was defined as 100%. The expression of treated cells was defined as the percentage relative to DMSO-treated cells. Values were analyzed with GraphPad Prism

https://doi.org/10.1021/acs.jmedchem.4c02577
J. Med. Chem. 2025, 68, 9202−9219

software using nonlinear regression analysis to determine DC_{50} and D_{max}.

Pharmacokinetics. Male CD-1(ICR) mice were dosed intraperitoneally with vehicle, YDR1, or YD54 at 1.25 mg/mL in 5% DMSO/5% solutol/90% water, final pH = 4.39 by pH meter, clear solution. NU/J nude mice were dosed oral gavage with vehicle (0.5% methylcellulose), YDR1 or YD54 at 1.25 mg/mL in 0.5% MC (4000 cps)/0.2% Tween 80 in water, homogeneous opaque suspension. Blood was collected to measure the mean plasma concentration of YDR1 and YD54. All blank matrix was freshly prepared. Protein precipitation (PPT) was done using a 96-well plate. An aliquot of 5 μL unknown sample, calibration standard, quality control, dilution quality control, single blank, and double blank samples were added to the 96-well plate, respectively. Each sample (except the double blank) was quenched with 200 μL of IS1 respectively (double blank sample was quenched with 200 μL of ACN), and then the mixture was vortex-mixed for 10 min at 800 rpm and centrifuged for 15 min at 3220 × *g*, 4 °C. An aliquot of 50 μL supernatant was transferred to another clean 96-well plate and centrifuged for 5 min at 3220 × *g*, 4 °C, and then the supernatant was directly injected for LC-MS/MS analysis.

Liver Microsomal Assays. Working solutions of the compound were prepared from 10 mM stock solution in dimethyl sulfoxide (DMSO) by diluting with 495 μL of acetonitrile (ACN) for intermediate solution concentration of 100 μM, 99% ACN. Using an Apricot automation workstation, 2 μL/well of compound working solution was added to all 96-well reaction plates except the blank (T0, T5, T15, T30, T45, T60, and NCF60). Then, an Apricot automation workstation was used to add 100 μL/well of microsome solution to all reaction plates (blank, T0, T5, T15, T30, T45, T60, and NCF60). All reaction plates containing mixtures of compound and microsomes were preincubated at 37 °C for 10 min. An Apricot automation workstation was used to add 98 μL/well of 100 mM potassium phosphate buffer to reaction plate NCF60. Reaction plate NCF60 was incubated at 37 °C for 1 h. After preincubation, 98 μL/well of NADPH regenerating system was added to every reaction plate except NCF60 (blank, T0, T5, T15, T30, T45, and T60) to start the reaction. Final concentration of each component in the incubation medium (0.5 mg protein/mL microsome, 1 mM test compound, 1 mM control compound, 10 mM ritonavir, 0.99% acetonitrile, 0.01% DMSO). The reaction plates were incubated at 37 °C. Six time points T0, T5, T15, T30, T45 and T60 min were included. An Apricot automation workstation was used to add 600 μL/well of stop solution (Cold (4 °C) acetonitrile (ACN) containing 200 ng/mL tolbutamide and 200 ng/mL labetalol as internal standards) followed by NADPH solution to each reaction plate at its appropriate end time point to terminate the reaction. Each plate was sealed and shaken for 10 min. After shaking, each plate was centrifuged at 4000 rpm and 4 °C for 20 min. After centrifugation, an Apricot automation workstation was used to transfer 300 μL of supernatant from each reaction plate to eight new 96-well plates for LC-MS/MS analysis. C_{max}, $T_{1/2}$, and AUC are calculated for liver microsomal assays. Assays were performed with a mouse liver microsome kit (Cat No. M1000), Xenotech.

Human Lung Xenografts Antitumor Efficacy Studies. All animal experiments were conducted in accordance with protocols reviewed and approved by the Institutional Animal Care and Use Committee at MDACC (00002017-RN01). To establish xenograft models, H1568 cells (2×10^6 cells/mouse), H2023 cells (10×10^6 cells/mouse), HCC515 cells (5×10^6 cells/mouse) and H2030 (10×10^6 cells/mouse) were trypsinized and resuspended in 1× PBS, mixed with a 1:1 mix of Matrigel in a final volume of 200 μL, and injected subcutaneously into the flanks of nude female mice (Jackson Laboratories) at 6−8 weeks of age. Tumor volume was measured by external caliper. Mice were randomized to control and treatment groups once the average tumor volume of H1568 xenograft reached 60 mm3 and H2023 xenograft, H2030 xenograft, and HCC515 tumor reached <200 mm^3, depending on the lung model. Vehicle, YDR1, and YD54 were prepared in 0.5% methylcellulose +0.2 to 1% Tween-80 solution by sonication. Briefly, freshly prepared solutions were subjected to six rounds of sonication: each pulse of 15 s with a gap of 2 min, while on ice. For H2030 xenograft experiments, vehicle and YD54 were prepared in 10% DMSO, 40% PEG300, 1% Tweeen-80, and 49% saline. Experimental mice were treated with vehicle, YDR1, or YD54 by oral gavage once daily until the end of the experiment. Tumor volume and mouse body weight were measured on alternate days. Tumor diameter and volume were calculated based on caliper measurements of tumor length and height using the formula tumor volume = (length × $width^2$)/2. The maximal tumor size permitted by our Institutional Animal Care and Use Committee is 2000 mm^3.

Quantitative Mass Spectrometry. *SMARCA4*-WT, H1792 cell line was treated with YDR1 48 h and submitted for multiplexed quantitative mass spectrometry analysis by Thermo Fisher Scientific Center for Multiplexed Proteomics (Harvard Medical School) processed and analyzed as previously described.[46] Sample processing steps included cell lysis, protein precipitation, tandem digestion with LysC and trypsin, peptide labeling with Tandem Mass Tag 6-plex reagents, and off-line bRP HPLC fractionation. Multiplexed quantitative mass spectrometry data was collected on an Orbitrap Fusion mass spectrometer operating in an MS3 mode using synchronous precursor selection for the MS2 to MS3 fragmentation.[47] MS/MS data were searched against a Uniport human database (February 2014) with SEQUEST using a target-decoy search strategy.[48] Data processing steps included controlling peptide and protein level false discovery rates, assembling proteins from peptides, and protein quantification from TMT reporter ions as previously described.[46]

Data Mining and Analysis. CRISPR/Cas9 knockout screening data were downloaded from the DepMap Public 23Q2 data set (https://depmap.org/portal/). Cell lines were called as *SMARCA4*-WT when SMARCA4 is free of mutation and *SMARCA4* mutant based on damaging mutations of *SMARCA4*.

Statistics and Reproducibility. GraphPad Prism 9 software was used to generate graphs and statistical analyses. Unpaired Student's *t* test determined statistical significance. Methods for statistical tests, the exact value of *n*, and the definition of error bars were shown in figure legends. All experiments have been reproduced in at least two independent experiments unless otherwise specified in the figure legends. All immunoblots and images shown are representatives of these independent experiments.

https://doi.org/10.1021/acs.jmedchem.4c02577
J. Med. Chem. 2025, 68, 9202−9219

■ ASSOCIATED CONTENT

Supporting Information

The Supporting Information is available free of charge at https://pubs.acs.org/doi/10.1021/acs.jmedchem.4c02577.

Experimental details for linker optimization and on-target activity of YDR1 and YD54, intracellular signaling pathway alterations, pharmcokinetics, and chemical synthetic procedures for YDR1 and YD54, and associated analytical data (1HNMR spectra & LCMS data) (PDF)

Molecular formula strings (CSV)

■ AUTHOR INFORMATION

Corresponding Author

Yonathan Lissanu − *Department of Thoracic and Cardiovascular Surgery, The University of Texas MD Anderson Cancer Center, Houston, Texas 77030, United states; Department of Genomic Medicine, The University of Texas MD Anderson Cancer Center, Houston, Texas 77030, United states;* orcid.org/0000-0003-1024-5303; Email: YLissanu@mdanderson.org

Authors

Sasikumar Kotagiri − *Department of Thoracic and Cardiovascular Surgery, The University of Texas MD Anderson Cancer Center, Houston, Texas 77030, United states*

Yawen Wang − *Department of Thoracic and Cardiovascular Surgery, The University of Texas MD Anderson Cancer Center, Houston, Texas 77030, United states*

Yanyan Han − *Department of Thoracic and Cardiovascular Surgery, The University of Texas MD Anderson Cancer Center, Houston, Texas 77030, United states*

Xiaobing Liang − *Department of Thoracic and Cardiovascular Surgery, The University of Texas MD Anderson Cancer Center, Houston, Texas 77030, United states*

Nicholas Blazanin − *Department of Thoracic and Cardiovascular Surgery, The University of Texas MD Anderson Cancer Center, Houston, Texas 77030, United states*

Hira Mazhar − *Department of Thoracic and Cardiovascular Surgery, The University of Texas MD Anderson Cancer Center, Houston, Texas 77030, United states*

Manu Sebastian − *Deptartment of Veterinary Medicine & Surgery and Department of Translational Molecular Pathology, The University of Texas MD Anderson Cancer Center, Houston, Texas 77030, United states*

Phuong Kieu Nguyen − *Institute for Applied Cancer Science, The University of Texas MD Anderson Cancer Center, Houston, Texas 77054, United states*

Yongying Jiang − *Institute for Applied Cancer Science, The University of Texas MD Anderson Cancer Center, Houston, Texas 77054, United states*

Complete contact information is available at: https://pubs.acs.org/10.1021/acs.jmedchem.4c02577

Author Contributions

S.K. designed the studies, interpreted the data, wrote some sections of the manuscript, and performed most of the experiments with assistance from Y.W, X.L., Y.H., H.M., and N.B. Y.W., Y.J., and P.K.N. performed the *in vivo* pharmacology experiments. S.K. and N.B. wrote the manuscript and formatted all figures. S.M. performed histopathology analysis. Y.L. conceived the work, designed the studies, designed PROTACs, oversaw the project, and wrote the manuscript. All authors commented on the paper.

Notes

The authors declare the following competing financial interest(s): Y.L. is an inventor on a patent application, WO 2023/129506 A1, for YD54, YDR1 and related compounds.

■ ACKNOWLEDGMENTS

We thank the MD Anderson Cancer Center (MDACC) Core facilities, including the histopathology core facility, and Shan Jiang for assistance with mouse colony maintenance. We also thank Dr Jack Roth and other members of the Department of Thoracic Surgery-Research section for valuable comments during the progress of this project. We thank Melinda Soeung, Jade Moehle, and Robert Nguyen for providing cell lines. This study was partly supported by the generous philanthropic contributions to The University of Texas MD Anderson Lung Cancer Moon Shots Program (Y.L.). This work is also supported by the University of Texas MD Anderson Cancer Center, Texas IGNITE (YL), and NIH grants R01CA272945 (YL) and R37CA251629 (YL).

■ ABBREVIATIONS USED

ATP, adenosine triphosphate; ATR, ataxia telangiectasia and rad3-related protein; *BRCA*, breast cancer; Cas9, crispr-associated protein 9; CRBN, cereblon; *CDKN2A*, cyclin-dependent kinase inhibitor 2A; ERK, extracellular signal-regulated kinase; EZH2, enhancer of zeste homologue 2; DC50, half-maximal degradation concentration; D_{max}, maximal degradation; DMSO, dimethyl sulfoxide; 1H NMR, proton nuclear magnetic resonance; HPLC, high-performance liquid chromatography; HAS, helicase-SANT-associated; KEAP1, kelch-like-associated protein 1; KRAS, kirsten rat sarcoma viral oncogene homologue; I.P, intraperitoneal injection; ICR, institute cancer research; LC-UV-HRMS, liquid chromatography with ultraviolet detection and high-resolution mass spectrometry; LC-MS/MS, liquid chromatography tandem mass spectrometry; MS, mass spectrometry; MAPK, mitogen-activated protein kinase; mg/kg, milligrams per kilogram; μM, micromolar; nM, nanomolar; NMR, nuclear magnetic resonance; NSCLC, nonsmall cell lung cancer; OS, overall survival; OXPHOS, oxidative phosphorylation; P.O, oral gavage; ppm, parts per million; PEG, polyethylene glycol; PROTAC, proteolysis-targeting chimeras; PARP, poly(ADP-ribose) polymerase; PFS, progression-free survival; PK, pharmacokinetic; WT, wild type; SEM, standard error of the mean; SNAr, nucleophilic aromatic substitution; TGI, tumor growth inhibition; SnAC, snf2 ATP coupling; TMT, tandem mass tag; SWI/SNF, switch/sucrose nonfermenting; VHL, von hippel lindau; YAP1, yes-associated protein 1

■ REFERENCES

(1) Errico, A. Genetics: SMARCA4 mutated in SCCOHT. *Nat. Rev. Clin Oncol* **2014**, *11* (6), 302.

(2) Cancer Genome Atlas Research Network. Comprehensive molecular profiling of lung adenocarcinoma. *Nature* **2014**, *511* (7511), 543−550.

(3) Kandoth, C.; McLellan, M. D.; Vandin, F.; Ye, K.; Niu, B.; Lu, C.; Xie, M.; Zhang, Q.; McMichael, J. F.; Wyczalkowski, M. A.; Leiserson, M. D. M.; Miller, C. A.; Welch, J. S.; Walter, M. J.; Wendl,

M. C.; Ley, T. J.; Wilson, R. K.; Raphael, B. J.; Ding, L. Mutational landscape and significance across 12 major cancer types. *Nature* **2013**, *502* (7471), 333−339.
(4) Lawrence, M. S.; Stojanov, P.; Mermel, C. H.; Robinson, J. T.; Garraway, L. A.; Golub, T. R.; Meyerson, M.; Gabriel, S. B.; Lander, E. S.; Getz, G. Discovery and saturation analysis of cancer genes across 21 tumour types. *Nature* **2014**, *505* (7484), 495−501.
(5) Varela, I.; Tarpey, P.; Raine, K.; Huang, D.; Ong, C. K.; Stephens, P.; Davies, H.; Jones, D.; Lin, M. L.; Teague, J.; Bignell, G.; Butler, A.; Cho, J.; Dalgliesh, G. L.; Galappaththige, D.; Greenman, C.; Hardy, C.; Jia, M.; Latimer, C.; Lau, K. W.; Marshall, J.; McLaren, S.; Menzies, A.; Mudie, L.; Stebbings, L.; Largaespada, D. A.; Wessels, L. F. A.; Richard, S.; Kahnoski, R. J.; Anema, J.; Tuveson, D. A.; Perez-Mancera, P. A.; Mustonen, V.; Fischer, A.; Adams, D. J.; Rust, A.; Chan-on, W.; Subimerb, C.; Dykema, K.; Furge, K.; Campbell, P. J.; Teh, B. T.; Stratton, M. R.; Futreal, P. A. Exome sequencing identifies frequent mutation of the SWI/SNF complex gene PBRM1 in renal carcinoma. *Nature* **2011**, *469* (7331), 539−542.
(6) Kadoch, C.; Hargreaves, D. C.; Hodges, C.; Elias, L.; Ho, L.; Ranish, J.; Crabtree, G. R. Proteomic and bioinformatic analysis of mammalian SWI/SNF complexes identifies extensive roles in human malignancy. *Nat. Genet.* **2013**, *45* (6), 592−601.
(7) Medina, P. P.; Romero, O. A.; Kohno, T.; Montuenga, L. M.; Pio, R.; Yokota, J.; Sanchez-Cespedes, M. Frequent BRG1/SMARCA4-inactivating mutations in human lung cancer cell lines. *Hum Mutat* **2008**, *29* (5), 617−622.
(8) Clapier, C. R.; Cairns, B. R. The biology of chromatin remodeling complexes. *Annu. Rev. Biochem.* **2009**, *78*, 273−304.
(9) Brownlee, P. M.; Meisenberg, C.; Downs, J. A. The SWI/SNF chromatin remodelling complex: Its role in maintaining genome stability and preventing tumourigenesis. *DNA Repair (Amst)* **2015**, *32*, 127−133.
(10) Lissanu Deribe, Y.; Sun, Y.; Terranova, C.; Khan, F.; Martinez-Ledesma, J.; Gay, J.; Gao, G.; Mullinax, R. A.; Khor, T.; Feng, N.; Lin, Y. H.; Wu, C. C.; Reyes, C.; Peng, Q.; Robinson, F.; Inoue, A.; Kochat, V.; Liu, C. G.; Asara, J. M.; Moran, C.; Muller, F.; Wang, J.; Fang, B.; Papadimitrakopoulou, V.; Wistuba, I. I.; Rai, K.; Marszalek, J.; Futreal, P. A. Mutations in the SWI/SNF complex induce a targetable dependence on oxidative phosphorylation in lung cancer. *Nat. Med.* **2018**, *24* (7), 1047−1057.
(11) Tagal, V.; Wei, S.; Zhang, W.; Brekken, R. A.; Posner, B. A.; Peyton, M.; Girard, L.; Hwang, T.; Wheeler, D. A.; Minna, J. D.; White, M. A.; Gazdar, A. F.; Roth, M. G. SMARCA4-inactivating mutations increase sensitivity to Aurora kinase A inhibitor VX-680 in non-small cell lung cancers. *Nat. Commun.* **2017**, *8*, 14098.
(12) Kim, K. H.; Kim, W.; Howard, T. P.; Vazquez, F.; Tsherniak, A.; Wu, J. N.; Wang, W.; Haswell, J. R.; Walensky, L. D.; Hahn, W. C.; Orkin, S. H.; Roberts, C. W. SWI/SNF-mutant cancers depend on catalytic and non-catalytic activity of EZH2. *Nat. Med.* **2015**, *21* (12), 1491−1496.
(13) Gupta, M.; Concepcion, C. P.; Fahey, C. G.; Keshishian, H.; Bhutkar, A.; Brainson, C. F.; Sanchez-Rivera, F. J.; Pessina, P.; Kim, J. Y.; Simoneau, A.; Paschini, M.; Beytagh, M. C.; Stanclift, C. R.; Schenone, M.; Mani, D. R.; Li, C.; Oh, A.; Li, F.; Hu, H.; Karatza, A.; Bronson, R. T.; Shaw, A. T.; Hata, A. N.; Wong, K. K.; Zou, L.; Carr, S. A.; Jacks, T.; Kim, C. F. BRG1 Loss Predisposes Lung Cancers to Replicative Stress and ATR Dependency. *Cancer Res.* **2020**, *80* (18), 3841−3854.
(14) Romero, O. A.; Vilarrubi, A.; Alburquerque-Bejar, J. J.; Gomez, A.; Andrades, A.; Trastulli, D.; Pros, E.; Setien, F.; Verdura, S.; Farré, L.; Martín-Tejera, J. F.; Llabata, P.; Oaknin, A.; Saigi, M.; Piulats, J. M.; Matias-Guiu, X.; Medina, P. P.; Vidal, A.; Villanueva, A.; Sanchez-Cespedes, M. SMARCA4 deficient tumours are vulnerable to KDM6A/UTX and KDM6B/JMJD3 blockade. *Nat. Commun.* **2021**, *12* (1), 4319.
(15) Rago, F.; DiMare, M. T.; Elliott, G.; Ruddy, D. A.; Sovath, S.; Kerr, G.; Bhang, H. C.; Jagani, Z. Degron mediated BRM/SMARCA2 depletion uncovers novel combination partners for treatment of BRG1/SMARCA4-mutant cancers. *Biochem. Biophys. Res. Commun.* **2019**, *508* (1), 109−116.
(16) Vangamudi, B.; Paul, T. A.; Shah, P. K.; Kost-Alimova, M.; Nottebaum, L.; Shi, X.; Zhan, Y.; Leo, E.; Mahadeshwar, H. S.; Protopopov, A.; Futreal, A.; Tieu, T. N.; Peoples, M.; Heffernan, T. P.; Marszalek, J. R.; Toniatti, C.; Petrocchi, A.; Verhelle, D.; Owen, D. R.; Draetta, G.; Jones, P.; Palmer, W. S.; Sharma, S.; Andersen, J. N. The SMARCA2/4 ATPase Domain Surpasses the Bromodomain as a Drug Target in SWI/SNF-Mutant Cancers: Insights from cDNA Rescue and PFI-3 Inhibitor Studies. *Cancer Res.* **2015**, *75* (18), 3865−3878.
(17) Farnaby, W.; Koegl, M.; Roy, M. J.; Whitworth, C.; Diers, E.; Trainor, N.; Zollman, D.; Steurer, S.; Karolyi-Oezguer, J.; Riedmueller, C.; Gmaschitz, T.; Wachter, J.; Dank, C.; Galant, M.; Sharps, B.; Rumpel, K.; Traxler, E.; Gerstberger, T.; Schnitzer, R.; Petermann, O.; Greb, P.; Weinstabl, H.; Bader, G.; Zoephel, A.; Weiss-Puxbaum, A.; Ehrenhofer-Wolfer, K.; Wohrle, S.; Boehmelt, G.; Rinnenthal, J.; Arnhof, H.; Wiechens, N.; Wu, M. Y.; Owen-Hughes, T.; Ettmayer, P.; Pearson, M.; McConnell, D. B.; Ciulli, A. BAF complex vulnerabilities in cancer demonstrated via structure-based PROTAC design. *Nat. Chem. Biol.* **2019**, *15* (7), 672−680.
(18) Hoffman, G. R.; Rahal, R.; Buxton, F.; Xiang, K.; McAllister, G.; Frias, E.; Bagdasarian, L.; Huber, J.; Lindeman, A.; Chen, D.; Romero, R.; Ramadan, N.; Phadke, T.; Haas, K.; Jaskelioff, M.; Wilson, B. G.; Meyer, M. J.; Saenz-Vash, V.; Zhai, H.; Myer, V. E.; Porter, J. A.; Keen, N.; McLaughlin, M. E.; Mickanin, C.; Roberts, C. W.; Stegmeier, F.; Jagani, Z. Functional epigenetics approach identifies BRM/SMARCA2 as a critical synthetic lethal target in BRG1-deficient cancers. *Proc. Natl. Acad. Sci. U. S. A.* **2014**, *111* (8), 3128−3133.
(19) Oike, T.; Ogiwara, H.; Tominaga, Y.; Ito, K.; Ando, O.; Tsuta, K.; Mizukami, T.; Shimada, Y.; Isomura, H.; Komachi, M.; Furuta, K.; Watanabe, S.; Nakano, T.; Yokota, J.; Kohno, T. A synthetic lethality-based strategy to treat cancers harboring a genetic deficiency in the chromatin remodeling factor BRG1. *Cancer Res.* **2013**, *73* (17), 5508−5518.
(20) Wilson, B. G.; Helming, K. C.; Wang, X.; Kim, Y.; Vazquez, F.; Jagani, Z.; Hahn, W. C.; Roberts, C. W. Residual complexes containing SMARCA2 (BRM) underlie the oncogenic drive of SMARCA4 (BRG1) mutation. *Mol. Cell. Biol.* **2014**, *34* (6), 1136−1144.
(21) Papillon, J. P. N.; Nakajima, K.; Adair, C. D.; Hempel, J.; Jouk, A. O.; Karki, R. G.; Mathieu, S.; Mobitz, H.; Ntaganda, R.; Smith, T.; Visser, M.; Hill, S. E.; Hurtado, F. K.; Chenail, G.; Bhang, H. C.; Bric, A.; Xiang, K.; Bushold, G.; Gilbert, T.; Vattay, A.; Dooley, J.; Costa, E. A.; Park, I.; Li, A.; Farley, D.; Lounkine, E.; Yue, Q. K.; Xie, X.; Zhu, X.; Kulathila, R.; King, D.; Hu, T.; Vulic, K.; Cantwell, J.; Luu, C.; Jagani, Z. Discovery of Orally Active Inhibitors of Brahma Homolog (BRM)/SMARCA2 ATPase Activity for the Treatment of Brahma Related Gene 1 (BRG1)/SMARCA4-Mutant Cancers. *J. Med. Chem.* **2018**, *61* (22), 10155−10172.
(22) Ottis, P.; Crews, C. M. Proteolysis-Targeting Chimeras: Induced Protein Degradation as a Therapeutic Strategy. *ACS Chem. Biol.* **2017**, *12* (4), 892−898.
(23) Kofink, C.; Trainor, N.; Mair, B.; Wohrle, S.; Wurm, M.; Mischerikow, N.; Roy, M. J.; Bader, G.; Greb, P.; Garavel, G.; Diers, E.; McLennan, R.; Whitworth, C.; Vetma, V.; Rumpel, K.; Scharnweber, M.; Fuchs, J. E.; Gerstberger, T.; Cui, Y.; Gremel, G.; Chetta, P.; Hopf, S.; Budano, N.; Rinnenthal, J.; Gmaschitz, G.; Mayer, M.; Koegl, M.; Ciulli, A.; Weinstabl, H.; Farnaby, W. A selective and orally bioavailable VHL-recruiting PROTAC achieves SMARCA2 degradation in vivo. *Nat. Commun.* **2022**, *13* (1), 5969.
(24) Cantley, J.; Ye, X.; Rousseau, E.; Januario, T.; Hamman, B. D.; Rose, C. M.; Cheung, T. K.; Hinkle, T.; Soto, L.; Quinn, C.; Harbin, A.; Bortolon, E.; Chen, X.; Haskell, R.; Lin, E.; Yu, S. F.; Del Rosario, G.; Chan, E.; Dunlap, D.; Koeppen, H.; Martin, S.; Merchant, M.; Grimmer, M.; Broccatelli, F.; Wang, J.; Pizzano, J.; Dragovich, P. S.; Berlin, M.; Yauch, R. L. Selective PROTAC-mediated degradation of

https://doi.org/10.1021/acs.jmedchem.4c02577
J. Med. Chem. 2025, 68, 9202−9219

SMARCA2 is efficacious in SMARCA4 mutant cancers. *Nat. Commun.* **2022**, *13* (1), 6814.
(25) Yang, L.; Tu, W.; Huang, L.; Miao, B.; Kaneshige, A.; Jiang, W.; Leng, L.; Wang, M.; Wen, B.; Sun, D.; Wang, S. Discovery of SMD-3040 as a Potent and Selective SMARCA2 PROTAC Degrader with Strong in vivo Antitumor Activity. *J. Med. Chem.* **2023**, *66* (15), 10761−10781.
(26) He, T.; Cheng, C.; Qiao, Y.; Cho, H.; Young, E.; Mannan, R.; Mahapatra, S.; Miner, S. J.; Zheng, Y.; Kim, N.; Zeng, V. Z.; Wisniewski, J. P.; Hou, S.; Jackson, B.; Cao, X.; Su, F.; Wang, R.; Chang, Y.; Kuila, B.; Mukherjee, S.; Dukare, S.; Aithal, K. B.; Samiulla, D. S.; Abbineni, C.; Vaishampayan, U.; Lyssiotis, C. A.; Parolia, A.; Xiao, L.; Chinnaiyan, A. M. Development of an orally bioavailable mSWI/SNF ATPase degrader and acquired mechanisms of resistance in prostate cancer. *Proc. Natl. Acad. Sci. U. S. A.* **2024**, *121* (15), No. e2322563121.
(27) Cieślak, M.; Słowianek, M. Cereblon-Recruiting PROTACs: Will New Drugs Have to Face Old Challenges? *Pharmaceutics* **2023**, *15* (3), 812.
(28) Zhang, L.; Riley-Gillis, B.; Vijay, P.; Shen, Y. Acquired Resistance to BET-PROTACs (Proteolysis-Targeting Chimeras) Caused by Genomic Alterations in Core Components of E3 Ligase Complexes. *Mol. Cancer Ther* **2019**, *18* (7), 1302−1311.
(29) Kotagiri, S.; Blazanin, N.; Xi, Y.; Han, Y.; Qudratullah; Liang, X.; Wang, Y.; Pandey, P.; Mazhar, H.; Lam, T. N.; Singh, A. K.; Wang, J.; Lissanu, Y. Enhancer reprogramming underlies therapeutic utility of a SMARCA2 degrader in SMARCA4 mutant cancer. *Cell Chem. Biol.* **2024**, 2069.
(30) Albrecht, B. K.Genetech Inc.,et al. Therapeutic pyridazine compounds and uses thereof. WO2016138114A1, Sept 1st, 2016.
(31) Desantis, J.; Mammoli, A.; Eleuteri, M.; Coletti, A.; Croci, F.; Macchiarulo, A.; Goracci, L. PROTACs bearing piperazine-containing linkers: what effect on their protonation state? *RSC Adv.* **2022**, *12* (34), 21968−21977.
(32) Zografou-Barredo, N. A.; Hallatt, A. J.; Goujon-Ricci, J.; Cano, C. A beginner's guide to current synthetic linker strategies towards VHL-recruiting PROTACs. *Bioorg. Med. Chem.* **2023**, *88*−*89*, No. 117334.
(33) Shah, P.; Westwell, A. D. The role of fluorine in medicinal chemistry. *J. Enzyme Inhib Med. Chem.* **2007**, *22* (5), 527−540.
(34) Kotagiri, S.; Blazanin, N.; Xi, Y.; Han, Y.; Qudratullah; Liang, X.; Wang, Y.; Pandey, P.; Mazhar, H.; Lam, T. N.; Singh, A. K.; Wang, J.; Lissanu, Y. Enhancer reprogramming underlies therapeutic utility of a SMARCA2 degrader in SMARCA4 mutant cancer. *Cell Chem. Biol.* **2024**, *31* (12), 2069−2084.e9.
(35) Hayhow, T. G.; Williamson, B.; Lawson, M.; Cureton, N.; Braybrooke, E. L.; Campbell, A.; Carbajo, R. J.; Cheraghchi-Bashi, A.; Chiarparin, E.; Diène, C. R.; Fallan, C.; Fisher, D. I.; Goldberg, F. W.; Hopcroft, L.; Hopcroft, P.; Jackson, A.; Kettle, J. G.; Klinowska, T.; Künzel, U.; Lamont, G.; Lewis, H. J.; Maglennon, G.; Martin, S.; Gutierrez, P. M.; Morrow, C. J.; Nikolaou, M.; Nissink, J. W. M.; O'Shea, P.; Polanski, R.; Schade, M.; Scott, J. S.; Smith, A.; Weber, J.; Wilson, J.; Yang, B.; Crafter, C. Metabolism-driven in vitro/in vivo disconnect of an oral ERa VHL-PROTAC. *Commun. Biol.* **2024**, *7* (1), 563.
(36) Fink, E. C.; McConkey, M.; Adams, D. N.; Haldar, S. D.; Kennedy, J. A.; Guirguis, A. A.; Udeshi, N. D.; Mani, D. R.; Chen, M.; Liddicoat, B.; Svinkina, T.; Nguyen, A. T.; Carr, S. A.; Ebert, B. L. Crbn (I391V) is sufficient to confer in vivo sensitivity to thalidomide and its derivatives in mice. *Blood* **2018**, *132* (14), 1535−1544.
(37) Gemechu, Y.; Millrine, D.; Hashimoto, S.; Prakash, J.; Sanchenkova, K.; Metwally, H.; Gyanu, P.; Kang, S.; Kishimoto, T. Humanized cereblon mice revealed two distinct therapeutic pathways of immunomodulatory drugs. *Proc. Natl. Acad. Sci. U. S. A.* **2018**, *115* (46), 11802−11807.
(38) Negrao, M. V.; Araujo, H. A.; Lamberti, G.; Cooper, A. J.; Akhave, N. S.; Zhou, T.; Delasos, L.; Hicks, J. K.; Aldea, M.; Minuti, G.; Hines, J.; Aredo, J. V.; Dennis, M. J.; Chakrabarti, T.; Scott, S. C.; Bironzo, P.; Scheffler, M.; Christopoulos, P.; Stenzinger, A.; Riess, J. W.; Kim, S. Y.; Goldberg, S. B.; Li, M.; Wang, Q.; Qing, Y.; Ni, Y.; Do, M. T.; Lee, R.; Ricciuti, B.; Alessi, J. V.; Wang, J.; Resuli, B.; Landi, L.; Tseng, S. C.; Nishino, M.; Digumarthy, S. R.; Rinsurongkawong, W.; Rinsurongkawong, V.; Vaporciyan, A. A.; Blumenschein, G. R.; Zhang, J.; Owen, D. H.; Blakely, C. M.; Mountzios, G.; Shu, C. A.; Bestvina, C. M.; Garassino, M. C.; Marrone, K. A.; Gray, J. E.; Patel, S. P.; Cummings, A. L.; Wakelee, H. A.; Wolf, J.; Scagliotti, G. V.; Cappuzzo, F.; Barlesi, F.; Patil, P. D.; Drusbosky, L.; Gibbons, D. L.; Meric-Bernstam, F.; Lee, J. J.; Heymach, J. V.; Hong, D. S.; Heist, R. S.; Awad, M. M.; Skoulidis, F. Comutations and KRASG12C Inhibitor Efficacy in Advanced NSCLC. *Cancer Discov* **2023**, *13* (7), 1556−1571.
(39) Genovese, G.; Carugo, A.; Tepper, J.; Robinson, F. S.; Li, L.; Svelto, M.; Nezi, L.; Corti, D.; Minelli, R.; Pettazzoni, P.; Gutschner, T.; Wu, C. C.; Seth, S.; Akdemir, K. C.; Leo, E.; Amin, S.; Molin, M. D.; Ying, H.; Kwong, L. N.; Colla, S.; Takahashi, K.; Ghosh, P.; Giuliani, V.; Muller, F.; Dey, P.; Jiang, S.; Garvey, J.; Liu, C. G.; Zhang, J.; Heffernan, T. P.; Toniatti, C.; Fleming, J. B.; Goggins, M. G.; Wood, L. D.; Sgambato, A.; Agaimy, A.; Maitra, A.; Roberts, C. W.; Wang, H.; Viale, A.; DePinho, R. A.; Draetta, G. F.; Chin, L. Synthetic vulnerabilities of mesenchymal subpopulations in pancreatic cancer. *Nature* **2017**, *542* (7641), 362−366.
(40) Meyers, R. M.; Bryan, J. G.; McFarland, J. M.; Weir, B. A.; Sizemore, A. E.; Xu, H.; Dharia, N. V.; Montgomery, P. G.; Cowley, G. S.; Pantel, S.; Goodale, A.; Lee, Y.; Ali, L. D.; Jiang, G.; Lubonja, R.; Harrington, W. F.; Strickland, M.; Wu, T.; Hawes, D. C.; Zhivich, V. A.; Wyatt, M. R.; Kalani, Z.; Chang, J. J.; Okamoto, M.; Stegmaier, K.; Golub, T. R.; Boehm, J. S.; Vazquez, F.; Root, D. E.; Hahn, W. C.; Tsherniak, A. Computational correction of copy number effect improves specificity of CRISPR-Cas9 essentiality screens in cancer cells. *Nat. Genet.* **2017**, *49* (12), 1779−1784.
(41) Ianevski, A.; Giri, A. K.; Aittokallio, T. SynergyFinder 3.0: an interactive analysis and consensus interpretation of multi-drug synergies across multiple samples. *Nucleic Acids Res.* **2022**, *50* (W1), W739−W743.
(42) Hendrick, C. E.; Jorgensen, J. R.; Chaudhry, C.; Strambeanu, I. I.; Brazeau, J. F.; Schiffer, J.; Shi, Z.; Venable, J. D.; Wolkenberg, S. E. Direct-to-Biology Accelerates PROTAC Synthesis and the Evaluation of Linker Effects on Permeability and Degradation. *ACS Med. Chem. Lett.* **2022**, *13* (7), 1182−1190.
(43) Troup, R. I.; Fallan, C.; Baud, M. G. J. Current strategies for the design of PROTAC linkers: a critical review. *Explor. Targeted Anti-Tumor Ther.* **2020**, *1* (5), 273−312.
(44) Bultman, S.; Gebuhr, T.; Yee, D.; La Mantia, C.; Nicholson, J.; Gilliam, A.; Randazzo, F.; Metzger, D.; Chambon, P.; Crabtree, G.; Magnuson, T. A Brg1 null mutation in the mouse reveals functional differences among mammalian SWI/SNF complexes. *Mol. Cell* **2000**, *6* (6), 1287−95.
(45) Holik, A. Z.; Krzystyniak, J.; Young, M.; Richardson, K.; Jarde, T.; Chambon, P.; Shorning, B. Y.; Clarke, A. R. Brg1 is required for stem cell maintenance in the murine intestinal epithelium in a tissue-specific manner. *Stem Cells* **2013**, *31* (11), 2457−66.
(46) Navarrete-Perea, J.; Yu, Q.; Gygi, S. P.; Paulo, J. A. Streamlined Tandem Mass Tag (SL-TMT) Protocol: An Efficient Strategy for Quantitative (Phospho)proteome Profiling Using Tandem Mass Tag-Synchronous Precursor Selection-MS3. *J. Proteome Res.* **2018**, *17* (6), 2226−2236.
(47) McAlister, G. C.; Nusinow, D. P.; Jedrychowski, M. P.; Wuhr, M.; Huttlin, E. L.; Erickson, B. K.; Rad, R.; Haas, W.; Gygi, S. P. MultiNotch MS3 enables accurate, sensitive, and multiplexed detection of differential expression across cancer cell line proteomes. *Anal. Chem.* **2014**, *86* (14), 7150−8.
(48) Elias, J. E.; Gygi, S. P. Target-decoy search strategy for mass spectrometry-based proteomics. *Methods Mol. Biol.* **2010**, *604*, 55−71.

https://doi.org/10.1021/acs.jmedchem.4c02577
J. Med. Chem. 2025, 68, 9202−9219